OPTIMIZATION OF A MEDIUM WITH LARGE PARAMETER OF NONLINEARITY AND ITS APPLICATION TO THE ENHANCEMENTOF A COMPACT, OMNIDIRECTIONAL, PARAMETRIC SOURCE

A Thesis
Presented to
The Academic Faculty

by

Etienne Dufour

In Partial Fulfillment
of the Requirements for the Degree
Master of Science in the
School of Mechanical Engineering

Georgia Institute of Technology
August 2006

OPTIMIZATION OF A MEDIUM WITH LARGE PARAMETER OF NONLINEARITY AND ITS APPLICATION TO THE ENHANCEMENTOF A COMPACT, OMNIDIRECTIONAL, PARAMETRIC SOURCE

Approved by:

Mr. David H. Trivett, Advisor
School of Mechanical Engineering
Georgia Institute of Technology

Dr. Peter H. Rogers, Advisor
School of Mechanical Engineering
Georgia Institute of Technology

Dr. Gerry H. Ginsberg
School of Mechanical Engineering
Georgia Institute of Technology

Date Approved: 05/18/06

ACKNOWLEDGEMENTS

I would like to express my deepest gratitude to all those who have assisted in the completion of this thesis. Foremost, I would like to thank my co-advisors, Mr. David H. Trivett, for his priceless advice and patient explanations, and Dr. Peter H Rogers, for his support throughout the duration of this project.

I would also like to thank Dr Jerry H. Ginsberg for serving on my thesis committee.

My gratitude is extended to Dr. François M. Guillot and Mr. John W. Doane for their help and availability.

TABLE OF CONTENTS

LIST OF FIGURES

SUMMARY

A compact low-frequency projector is of crucial importance especially in underwater acoustics due to the frequency dependence of the absorption.

To improve the efficiency of an omnidirectional acoustic source at low frequencies, parametric amplification may be used by adding a thin layer of nonlinear medium around a spherical transducer.

The parametric effect is based on the interaction of two acoustic waves propagating through a nonlinear medium to produce a difference frequency wave. If both primary frequencies are sufficiently close enough, the result is the creation of a low frequency wave. Investigation is required to find the optimal medium, that is to say, one with a large nonlinear coefficient and a low sound speed. Such a source has already been built using a medium composed of a gel and microsphere mixture. In this case, the nonlinear coefficient is highly pressure dependent reaching a maximum when the microspheres buckle. The need is to optimize the material layer to increase the range of hydrostatic pressures over which the projector is useful.

CHAPTER I

INTRODUCTION

1.1 Background

Propagation of sound through water has been studied for a long time. Advantages of water propagation over air propagation include higher speed and the possibility of long distance transmissions. As is the case for all media, sound propagation in water depends on frequency. Sound waves propagating through a medium are subject to attenuation. In the case of water, absorption is due to both viscosity and thermal conductivity and is in general, proportional to the square of frequency. This means that high frequency components of a signal are damped much faster than low frequency waves, the latter remain in the far-field. Long distance signal transmission can therefore only be achieved with low frequency sound waves.

However, low frequency is associated with of large displacements which are difficult to generate with piezoelectric transducers due to the resonant frequency generally being relatively high.

One way to overcome this problem is to use parametric amplification, which can be defined as the generation of a low difference frequency wave from the nonlinear interaction of two high frequency primaries. This nonlinear effect was first described theoretically by Westervelt in 1963 [1]. Experimental verifications were performed by Berktay in 1965 [2]. A numerical solution to Westervelt's theory was presented by Muir

and Willette in 1972 [3]. A main disadvantage with the parametric array was its low efficiency. To date, this problem has prevented the wide spread application of the parametric array underwater. To address this problem, researchers have focused on the enhancement of the nonlinear coefficient of the medium contained in the parametric array. In 1980, Woodsum [4] suggested the use of air bubbles in water. Experimental verifications were conducted [5] and followed by investigations of bubble layers [6, 7 and 8]. In these studies, nonlinear vibration of the air bubbles at their resonance frequency is responsible for nonlinear enhancement. This occurs when the primary wave frequencies match the resonant frequencies of the bubbles, which requires uniform bubble size. Additional enhancement can be obtained by designing the bubble layer thickness to be resonant at the difference frequency [9]. In this case, the bubbles compliance decreases the sound speed in the layer resulting in both an impedance mismatch with the surrounding medium and an effective increase in the thickness. In addition to the difficulty of producing uniform bubbles, the instability of free bubbles in water remained an issue.

More recently, Asada and Watanabe [11] proposed the use of microcapsules in a silicone rubber in order to provide a more stable medium. Their goal was also to create nonlinearities from the vibration of the microcapsules at high frequencies.

This work follows previous efforts at the Georgia Institute of Technology. H. Pinçon [23] and O.Pauli [24] investigated a medium with a large nonlinear coefficient. Unlike bubbly media, this work uses a low-frequency effect. The medium they investigated was composed of castor oil and Expancel® microspheres and the high levels of nonlinearity were due to the buckling and unbuckling of the microspheres resulting in a change in

compliance of the medium as an acoustic wave propagates. A. Dumortier [25] used their results to design and build an omnidirectional parametric projector with a nonlinear layer made of microspheres and Xanthan gel. He succeeded in generating high levels of difference frequency but the enhancement occurred over a limited range of depths.

Based on these previous studies, the goal of this investigation is to extend operational range of depths over which a compact source will produce high levels of difference frequency, and replace the Xanthan gel with a solid material to improve handling.

1.2 Thesis objectives

The feasibility of an efficient compact, omnidirectional parametric source has been demonstrated [25]. However, limited hydrostatic pressure range and delicate handling requirements appeared to be obstacles for practical use and design improvements are therefore needed.

Implementation of these improvements requires the following steps:

- Development for a nonlinear medium that reduces handling issues and extends the efficient range of use to a broader range of hydrostatic pressures.

- Predict performance of the medium when used as a nonlinear layer for a parametric projector. This aspect requires practical determination of the medium properties (sound speed and nonlinear coefficient) and simulation of a sound wave traveling trough this medium.

- Build a source with the newly developed medium and perform measurements to determine the amplitude of the difference frequency component.

1.3 Organization of the thesis

The second chapter presents the theoretical basis of nonlinear acoustics and presents the general equations that describe the behavior of a sound wave propagating through a nonlinear medium.

The third chapter describes a parametric array and the enhancement of the low-frequency signal due to the resonance of the material layer. A method to simulate the sound wave propagation through a nonlinear medium is also presented.

The fourth chapter describes the different parameters of the nonlinear medium and their role in the parametric mechanism. Results of the measurements that lead to the different choices are also reported.

The fifth chapter is devoted to the description of the different steps of the assembly of the nonlinear layer on the piezoelectric source.

The sixth chapter is dedicated to the practical measurements, obtained in the water tank and the pressure chamber, and their results.

Finally, the seventh chapter concludes the thesis by summarizing the work carried out and the obtained results. Work perspectives are also offered.

CHAPTER II

THEORETICAL BACKGROUND

Sound can be defined as the propagation of a perturbation through a medium. To understand phenomena occurring during the propagation, equations modeling the theory of motion of a fluid are studied.

2.1 Basic Equations

2.1.1 The mass conservation, or continuity, equation

Conservation of the mass of a fluid can be obtained by equating the time rate of change of mass in an arbitrary fixed volume V bounded by a surface S to the mass flux per unit time through the surface S

$$\frac{\partial}{\partial t}\int_V \rho dV = -\int_S \rho \mathbf{v}.d\mathbf{S} \tag{2.1}$$

where, ρ is the density of the medium, and, v is the fluid particle velocity.

Gauss' theorem gives us:

$$\frac{\partial}{\partial t}\int_V \rho dV = -\int_V \nabla\cdot(\rho \boldsymbol{v})dV\,. \tag{2.2}$$

Since the volume V is arbitrary, the integrand must vanish and we obtained the mass conservation equation:

$$\frac{\partial \rho}{\partial t} + \nabla\cdot(\rho \boldsymbol{v}) = 0\,. \tag{2.3}$$

2.1.2 The Navier-Stokes equation of motion

This equation, which is also called conservation of momentum, takes into account the dissipation due to viscosity or thermal conduction. The starting point is the same as equation (2.1) except that ρ is replaced by $\rho \boldsymbol{v}$ and that the volume and surface forces exerted on the fluid in the volume *V* are added:

$$\int_S \rho v_i v_k dS_k - \int_V \rho f_i dV - \int_S \sigma_{ik} dS_k = -\frac{\partial}{\partial t}\int_V \rho v_i dV \tag{2.4}$$

With,

$$\sigma_{ik} = -p\delta_{ik} + \mu\left(\frac{\partial v_i}{\partial x_k} + \frac{\partial v_k}{\partial x_i} - \frac{2}{3}\frac{\partial v_r}{\partial x_r}\delta_{ik}\right) + \frac{2}{3}\lambda\frac{\partial v_r}{\partial x_r}\delta_{ik}\ , \tag{2.5}$$

where δ_{ik} is the Kronecker tensor, μ and λ the viscosity coefficients.

Applying Gauss' theorem yields

$$\frac{\partial}{\partial t}(\rho v_i)+\frac{\partial}{\partial x_k}(\rho v_i v_k)=\rho f_i+\frac{\partial}{\partial x_k}(\sigma_{ik})\ . \tag{2.6}$$

Setting $f=0$, $\mu=\eta$, $\frac{2}{3}\lambda=\zeta$, we finally obtain the Navier-Stock equation

$$\rho(\frac{\partial \vec{v}}{\partial t}+\boldsymbol{v}\cdot\nabla\boldsymbol{v})=-\nabla p+\eta\Delta\boldsymbol{v}+(\zeta+\frac{\eta}{3})\nabla(\nabla\cdot\boldsymbol{v}) \tag{2.7}$$

where ζ is the bulk viscosity and η the shear viscosity.

2.1.3 The heat transfer equation

The energy in a fixed volume V can be reduced by three ways. The net internal energy flow from V through its surface S because of fluid motion; the net heat flow out from V through S and the work done per time by the fluid in the volume on its surroundings. This can be expressed by the following equation

$$\int_S \rho u v_i dS_i+\int_S q_i dS_i-\int_S v_i\sigma_{ik}dS_k=-\frac{\partial}{\partial t}\int_V \rho u dV \tag{2.8}$$

with u the total energy per mass and q_i the heat flow density. After several steps [26], the heat transfer equation is obtained

$$\rho T\left[\frac{\partial s}{\partial t}+(\boldsymbol{v}\cdot\nabla)s\right]=\kappa\Delta T+\zeta(\nabla\cdot\boldsymbol{v})^2+\frac{1}{2}\eta\left(\frac{\partial v_i}{\partial x_j}+\frac{\partial v_j}{\partial x_i}-\frac{2}{3}\nabla\cdot\boldsymbol{v}\delta_{ij}\right)^2, \tag{2.9}$$

which expresses the conservation of energy. Here, T is the temperature, s, the entropy and, κ is the heat conduction number.

2.2 Lossless Theory

We now consider small acoustical perturbations in an ideal fluid.

$$p' = p - p_0 \tag{2.10}$$

$$\rho' = \rho - \rho_0 \tag{2.11}$$

Which means that the acoustic pressure and density are considered as fluctuations about an equilibrium state. Neglecting second and higher order terms due to the small perturbation approximation, the Navier-Stokes equation (2.7) reduces to the linearized equation of motion

$$\rho_0 \frac{\partial v}{\partial t} + \nabla p' = 0 . \tag{2.12}$$

Equation (2.3) becomes

$$\frac{\partial \rho'}{\partial t} + \rho_0 \nabla \cdot v . \tag{2.13}$$

The adiabatic equation of state is then

$$p' = c_0^2 \rho', \; c_0^2 = \left(\frac{\partial p}{\partial \rho} \right)_s . \tag{2.14}$$

Equations (2.12), (2.13) and (2.14) can be regrouped in a single equation by introducing a velocity potential φ defined by $v = \nabla \varphi$ resulting in

$$\frac{\partial^2 \varphi}{\partial t^2} - c_0^2 \nabla^2 \varphi = 0 \tag{2.15}$$

This is the well-known linear equation of propagation. The general solution of Eq. (2.15) is of the form:

$$\varphi = F(x - ct) + G(x + ct), \tag{2.16}$$

Where F and G are arbitrary functions. This solution represents the propagation of two linear sound waves in opposite directions.

2.3 Introduction of nonlinearity

A Taylor series expansion of the pressure, in terms of the density, of the equation of state yields:

$$p = p_0 + \left(\frac{\partial p}{\partial \rho}\right)_{s,\rho=\rho_0} (\rho - \rho_0) + \frac{1}{2}\left(\frac{\partial^2 p}{\partial \rho^2}\right)_{s,\rho=\rho_0} (\rho - \rho_0)^2 + \ldots \tag{2.17}$$

which may be rewritten as,

$$= p_0 + A\frac{\rho'}{\rho_0} + \frac{1}{2}B\left(\frac{\rho'}{\rho_0}\right)^2, \tag{2.18}$$

where

$$A = \rho_0\left(\frac{\partial p}{\partial \rho}\right)_{s,\rho=\rho_0} = \rho_0 c_0^2 \tag{2.19}$$

$$B = \rho_0^2\left(\frac{\partial^2 p}{\partial \rho^2}\right)_{s,\rho=\rho_0} \tag{2.20}$$

In most cases, terms higher than the second order are not necessary.

The ratio B/A of the nonlinear and linear coefficient of the equation of state characterizes the thermodynamic nonlinearity of the medium.

$$\frac{B}{A} = \frac{\rho_0}{c_0^2}\left(\frac{\partial^2 p}{\partial \rho^2}\right)_{s,\rho=\rho_0} = 2\rho_0 c_0\left(\frac{\partial c}{\partial p}\right)_{s,\rho=\rho_0} \tag{2.21}$$

The coefficient B/A physically represents the variation of the medium sound speed induced by a change of the total pressure.

2.4 Equations of propagation

By keeping all the terms of the basic equations (2.3, 2.7, 2.9 and the equation of state), we obtain the equation derived by Kuznetsov (1971)

$$\nabla^2\varphi - \frac{1}{c_0^2}\frac{\partial^2\varphi}{\partial t^2} = \frac{1}{c_0^2}\frac{\partial}{\partial t}\left[(\nabla\varphi)^2 + \frac{\gamma-1}{2c_0^2}\left(\frac{\partial\varphi}{\partial t}\right)^2 + \frac{b}{\rho_0}\Delta\varphi\right], \tag{2.22}$$

where $\gamma = \frac{C_p}{C_v}$ and b is defined as $b = \kappa\left(\frac{1}{C_v} - \frac{1}{C_p}\right) + \frac{4}{3}\eta + \xi$.

Assuming plane waves and slow changes of the wave profile, we can make the following change of variables

$x' = \mu x$, with μ small

$\tau = t - \frac{x}{c_0}$.

Consequently, we obtain:

$$\frac{\partial}{\partial x} = -\frac{1}{c_0}\frac{\partial}{\partial\tau} + \mu\frac{\partial}{\partial x'} \tag{2.23}$$

$$\frac{\partial}{\partial t} = \frac{\partial}{\partial\tau}. \tag{2.24}$$

Assuming that b and φ are small and retaining only second order terms, equation (2.22) becomes

$$2\mu c_0 \frac{\partial^2 \varphi}{\partial \tau \partial x'} = \frac{1}{c_0^2} \frac{\partial}{\partial \tau} \left[\left(\frac{\partial \varphi}{\partial \tau} \right)^2 + \frac{\gamma - 1}{2} \left(\frac{\partial \varphi}{\partial t} \right)^2 + \frac{b}{\rho_0} \frac{\partial^2 \varphi}{\partial \tau^2} \right]. \tag{2.25}$$

In terms of fluid velocity, recalling that $v = -\frac{\partial \varphi}{\partial x} = \frac{1}{c_0} \frac{\partial \varphi}{\partial \tau}$,

$$\frac{\partial v}{\partial x} - \frac{\beta}{c_0^2} v \frac{\partial v}{\partial \tau} = \frac{b}{2 c_0^3 \rho_0} \frac{\partial^2 v}{\partial \tau^2}, \tag{2.26}$$

with $\beta = 1 + \frac{B}{2A}$, the nonlinearity parameter.

This last equation is known as Burgers' equation (Burgers, 1948)

2.5 Distortion

In the previous section, we showed that the propagation of an acoustic plane wave can be described by Burger's equation. If we neglect dissipation, Burgers' equation reduces to

$$\frac{\partial v}{\partial x} - \frac{\beta}{c_0^2} v \frac{\partial v}{\partial \tau} = 0. \tag{2.27}$$

The solution of this equation is of the form

$$v = F\left(\tau + \frac{\beta}{c_0^2} vx \right), \tag{2.28}$$

where F is an arbitrary function. Recalling that $\tau = t - \frac{x}{c_0}$, we get

$$v = F\left(t - \frac{x}{c_0} + \frac{\beta}{c_0^2} vx \right) \tag{2.29}$$

then

$$\Delta t = \frac{\Delta x}{c_0}\left(1 - \frac{\beta}{c_0} v \right) \tag{2.30}$$

so

$$c = \frac{\Delta x}{\Delta t} = c_0\left(1 - \frac{\beta}{c_0} v \right)^{-1} \approx c_0\left(1 + \frac{\beta}{c_0} v \right) = c_0 + \beta v \tag{2.31}$$

Equation (2.30) indicates that each point of the wave profile travels at a different speed, as illustrated in Fig. 2.1.

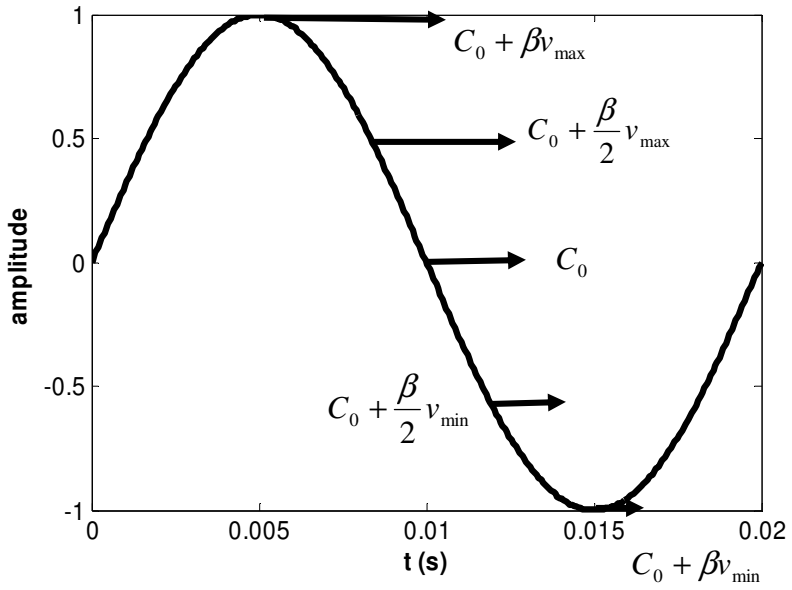

Figure 2.1-Sound speed variations along a wave profile

This results in a progressive distortion of the wave profile. The amount the wave is distorted depends on the nonlinear coefficient β, and the direction in which the waveform distorts depends on the sign of β.

a) The positive coefficient of nonlinearity

When β is positive, the speed of sound increases with increasing pressure. The positive portion of the wave profile, which corresponds to the compression phase, travels faster than the negative portion, which corresponds to the decompression phase. So, one part of the wave travels at a supersonic speed while the other travels at subsonic speed. This results in a progressive and cumulative distortion of the wave. When the positive overpressure approaches the negative depression, the shock or discontinuity distance has

been reached. The wave profile is then called N-wave due to its shape. After this point, the wave cannot distort further, otherwise it would allow the formation of a multivalued wave profile which is physically impossible. This is illustrated on Fig. 2.2, where the wave is moving to the left-hand side.

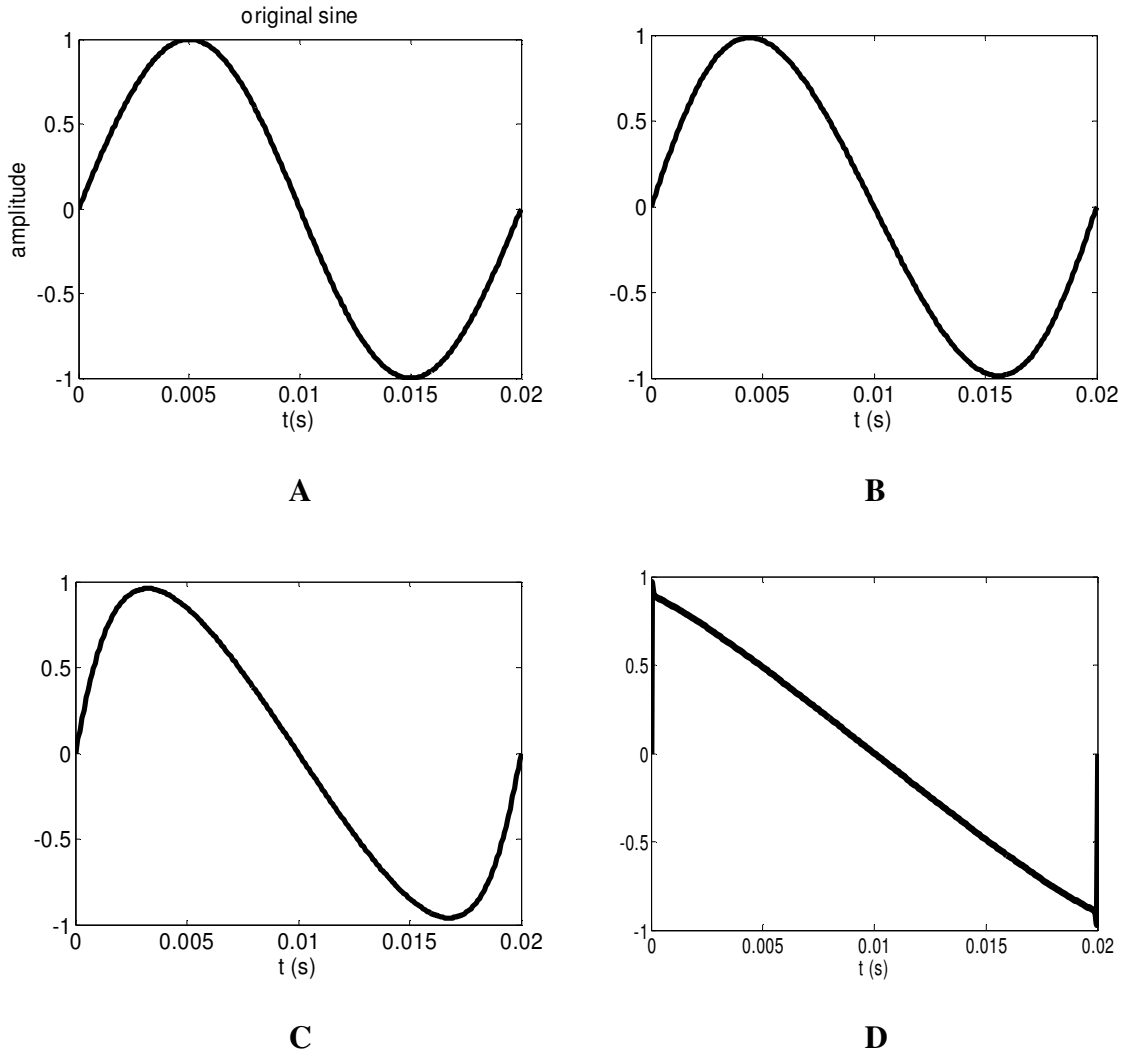

Figure 2.2- Wave distortion during the propagation through a medium with a positive nonlinear coefficient. a) Initially sinusoidal, b) Early distortion, c) Moderate distortion, d) N-wave

b) The negative coefficient of nonlinearity

When β is negative, the speed of sound decreases with an increase in pressure so that the distortion leads to a rarefaction shockwave and to the formation of a sawtooth shape wave, as illustrated in Fig.2.3. The discontinuity of the function means that there is a sudden change of pressure, which explains the term "shock".

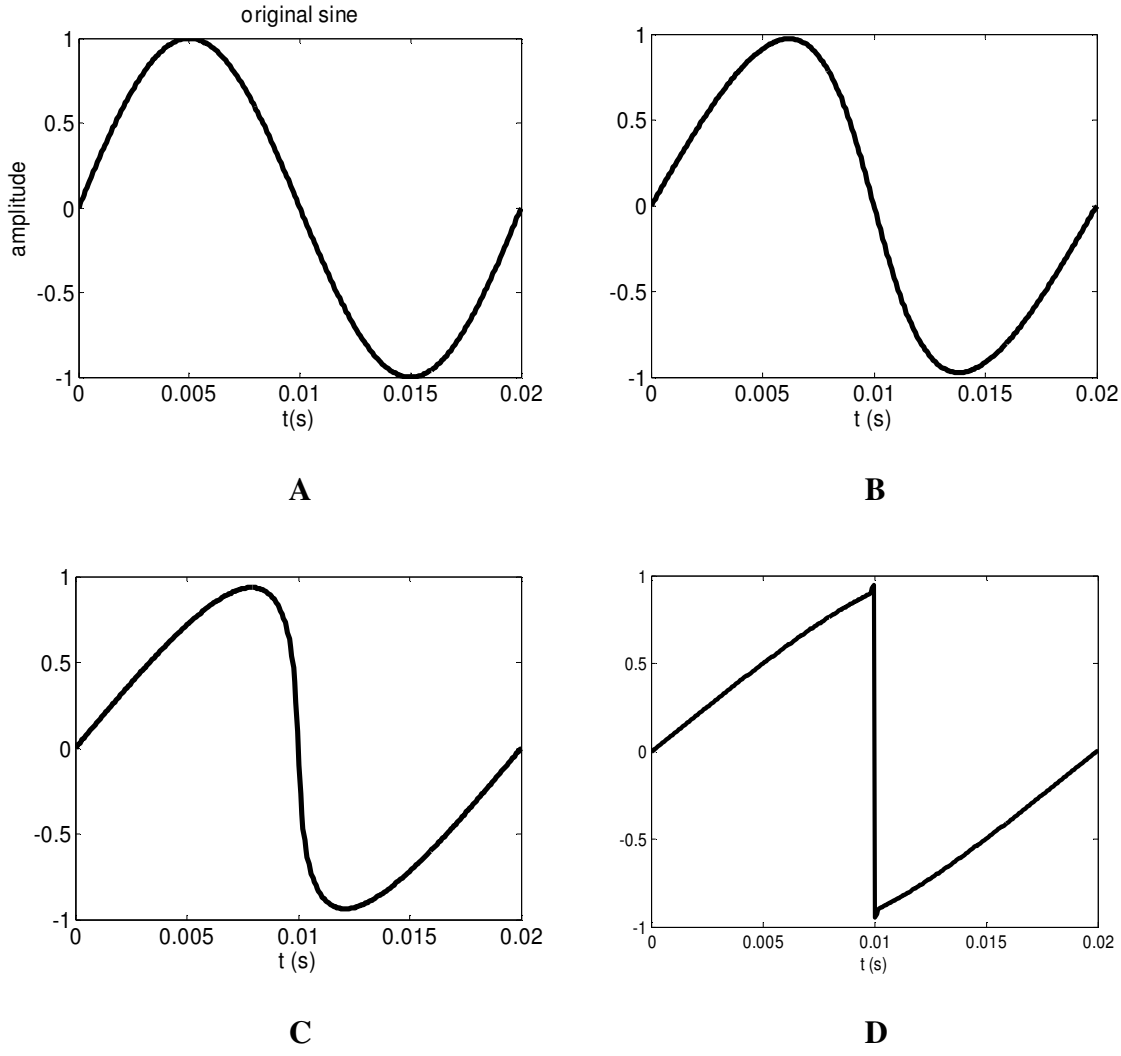

Figure 2.3- Wave distortion during the propagation through a medium with a negative nonlinear coefficient. a) Initially sinusoidal, b) Early distortion, c) Moderate distortion, d) Sawtooth

Distortion of the waveform may also be described as the generation of harmonics of the initially sinusoidal primary wave. At the start, the signal is composed of a pure sine; only one frequency component is present. As the waveform propagates, a second harmonic component is generated from the interaction of the fundamental with itself. The second interacts with the fundamental to produce the third and so on. Ultimately, if the attenuation is low enough, high levels of all harmonics are present. Generation of the harmonics can also be observed by Fourier transforming the different waveforms. Thus, on one hand distortion implies the creation of harmonics of the primary frequency; on the other hand, absorption due to viscosity and thermal conductivity, which is, in general, proportional to the square of frequency, attenuates these harmonics. We therefore have two competing phenomena as sketched on Fig. 1.4. It has to be noted that the absorption also reduces the wave amplitude.

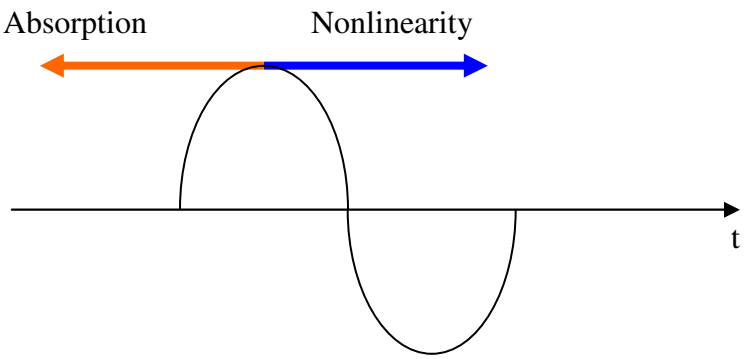

Figure 2.4- Nonlinearity and dissipation

2.6 Transfer of energy

The distortion process can also be studied in the frequency domain. When the wave is distorted, harmonics are created, which means that part of the energy of the primary wave is transferred to harmonics during the propagation. This can be verified, numerically, by sending a sinusoidal signal through a nonlinear medium and observing the amplitudes of the different harmonics as a function of the propagation distance. In figure 2.5, the levels of the first four harmonics are plotted; the nonlinear parameter β and the sound speed c of the medium are arbitrarily taken.

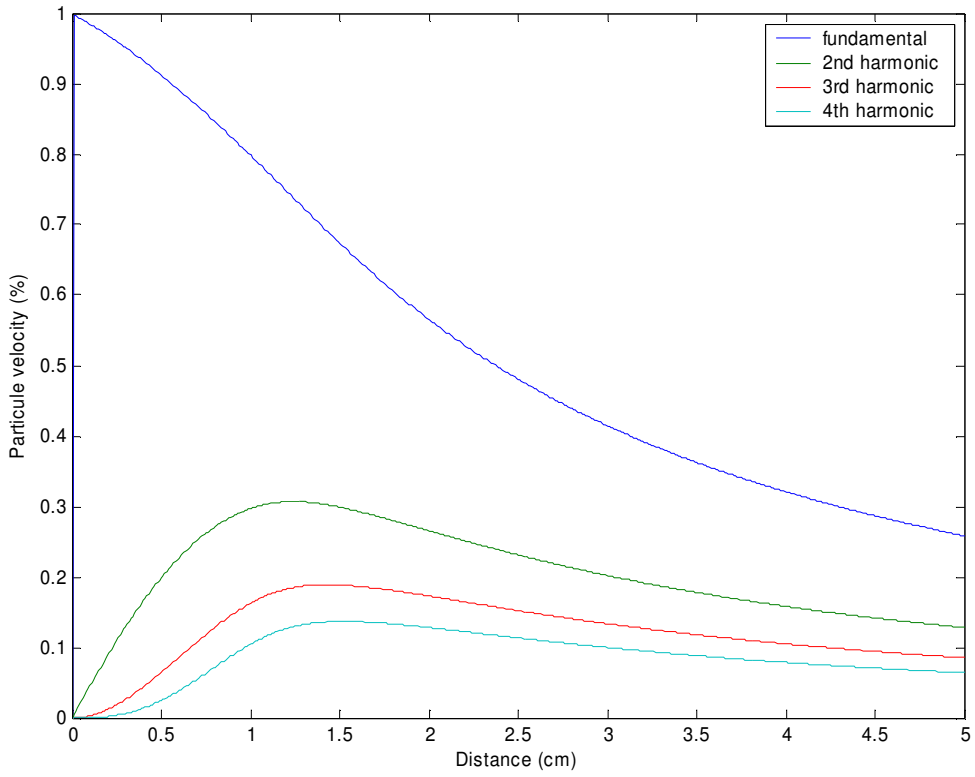

Figure 2.5- Changes of amplitude due to the energy transfer during the propagation of a pure tone signal at 300Hz through a nonlinear medium ($\beta = 500$; $c = 100$)

At the beginning of the propagation, the amplitude of the fundamental drops as energy flows into the harmonics. The rate of energy conversion largely depends on the nonlinear coefficient which explains the importance of the nonlinear medium in the parametric amplification. As the signal continues to propagate, the amplitude of the harmonics reaches a maximum and eventually decreases due to spherical spreading and linear attenuation. The energy in the fundamental becomes eventually too small to compensate for losses.

CHAPTER III

SOURCE DESCRIPTION AND PROPAGATION SIMULATION

This chapter presents the principles on which the source design is based. First, the concept of a parametric array is described; then a program to simulate propagation of a wave through such an array is presented.

3.1 Parametric array

A parametric array relies on the interaction between two different waves propagating in the same direction through a nonlinear medium. These primary waves interact with each other as they propagate through the medium, leading to the generation of difference and sum frequency waves, as well as harmonics of the primary waves. In most cases, the frequency dependence of the viscous absorption is quadratic. The high frequency waves are therefore damped rapidly and it is the difference frequency wave that is mainly transmitted to the external medium.

3.2 Model description

In this work, a model previously utilized by Dumortier [25] is used to predict the acoustic pressure produced by the source at the difference frequency. Due to the mismatch of impedance at the medium-water interface medium-water, reflections occur and may lead to a resonance phenomenon. To compute the contribution of this resonance, one should first calculate the propagation of the wave through the nonlinear medium and determine the transmitted and reflected components of the difference frequency at the material/fluid boundary. It is then necessary to propagate the reflected wave back to the source, reflect it, and propagate back out to the material/fluid interface; this process the needs to be repeated. Furthermore, such an analysis would need to account for the nonlinear interaction between the inward and outward waves. Performing this analysis would be quite difficult. We therefore use an approximate approach, propagating the wave outward nonlinearly and using spherical waves but considering only plane waves and linear medium for the reflections. This alternative gives a good approximation because the attenuation of primary frequency wave amplitudes from the inner to the outer radius is such that the generation of the difference frequency after reflection is negligible. In our case, this attenuation is approximately 15 dB. The simulation through the nonlinear medium is then done only for one direction. The gain due to the resonance effect is then determined linearly by using plane waves. One should also note that the model does not take into account the possible nonlinearities due to nonlinear vibrations of the thick shell composed of the transducer and the nonlinear layer.

3.3 Computation

In order to make theoretical predictions about the efficiency of a parametric source, we need to simulate the propagation of a wave through a nonlinear medium. To do this, several kinds of algorithms have been developed:

- Time-domain algorithms where all the calculations are preformed in the time domain. This method is based on the Nonlinear Progressive wave Equation (NPE) [20].

- Frequency-domain algorithms where all the calculations are performed in the frequency domain. This type of programs requires the computation of a large number of harmonics, especially in the case of absorption coefficients [15].

- Hybrid algorithms where the nonlinear steepening is performed in the time domain but where absorption and diffraction are computed in the frequency domain. The main problem with this kind of algorithms is the need to switch all the time from one domain to another, which is time-consuming [21].

In our case, a frequency-domain algorithm is used. This program has been developed by Trivett and Van Buren [15]. In this algorithm, the wave propagation is divided in small intervals. The distortion is first calculated over a small interval then the amplitude is

corrected to take into account absorption and geometrical spreading and dispersion, if present. The size of the interval has to be small enough in order for the change introduced by each mechanism remains small and to allow the interaction between them. A copy of this algorithm is provided in appendix (Appendix I).

3.3.1 Theory

Starting with Burger's equation

$$\frac{\partial v}{\partial r} - \frac{\beta}{c_0^2} v \frac{\partial v}{\partial \tau} = \frac{b}{2c_0^3 \rho_0} \frac{\partial^2 v}{\partial \tau^2}, \tag{3.1}$$

where r is the distance from the center of the source.

We removes the quadratic term of losses, to replace it by a more general equation, Eq. (3.13) reduces to

$$\frac{\partial v}{\partial r} - \frac{\beta}{c_0^2} v \frac{\partial v}{\partial \tau} = 0. \tag{3.2}$$

Then to generalize to all types of wave, we introduce a third term that represents geometrical spreading

$$\frac{\partial v}{\partial r} + \left(\frac{a}{r}\right) v - \frac{\beta}{c_0^2} v \frac{\partial v}{\partial \tau} = 0, \tag{3.3}$$

With a =0 for plane waves

=1/2 for cylindrical waves

=1 for spherical waves

Finally, linear absorption is taken into account as follows

$$\frac{\partial v}{\partial r}+\left(\frac{a}{r}\right)v-\frac{\beta}{c_0^2}v\frac{\partial v}{\partial \tau}=-\alpha(w)v\,. \tag{3.4}$$

We need a solution of equation (3.16). This can be accomplished by first introducing a general solution of the form:

$$v(r,\tau)=\sum_{k=1}^{\infty}\left(\frac{r_0}{r}\right)^a\{G_k\sin(kw_0\tau)+H_k\cos(kw_0\tau)\}\exp[-\alpha_k(r-r_0)]\,, \tag{3.5}$$

Where, α_k is the absorption coefficient corresponding to the k^{th} element. Substituting Eq. (3.5) into equation (3.4) yields two coupled differential equations

$$\frac{\partial G_k}{\partial r} = \frac{\beta\omega_0}{2{c_0}^2}\left(\frac{r_0}{r}\right)^a \left\{\sum_{m=1}^{k-l} m\left(G_{k-m}G_m - H_{k-m}H_m\right).\exp\left[-\left(\alpha_{k-m} + \alpha_m - \alpha_k\right)\left(r - r_0\right)\right]\right.$$

$$\left. - k\sum_{m=1}^{\infty}\left(G_{k+m}G_m + H_{k+m}H_m\right).\exp\left[-\left(\alpha_{k+m} + \alpha_m - \alpha_k\right)\left(r - r_0\right)\right]\right\} \tag{3.6}$$

$$\frac{\partial H_k}{\partial r} = \frac{\beta\omega_0}{2{c_0}^2}\left(\frac{r_0}{r}\right)^a \left\{\sum_{m=1}^{k-l} m\left(H_{k-m}G_m - H_m G_{k-m}\right).\exp\left[-\left(\alpha_{k-m} + \alpha_m - \alpha_k\right)\left(r - r_0\right)\right]\right.$$

$$\left. + k\sum_{m=1}^{\infty}\left(H_m G_{k+m} - H_{k+m}G_m\right).\exp\left[-\left(\alpha_{k+m} + \alpha_m - \alpha_k\right)\left(r - r_0\right)\right]\right\} \tag{3.7}$$

These equations can be solved numerically to yield the harmonic amplitudes G_k and H_k. In order to perform this computation, the series need to be truncated to a finite number of terms.

A potential problem with the truncation is that it can cause the energy in the last harmonics being too high, leading to numerical instability due to the absence of energy transfer to higher harmonics. To prevent this problem, the energy of the last harmonics is artificially reduced by keeping their amplitudes lower than the previous one.

The integration is then implemented using a Runge-Kutta method [31]. The amplitude of the harmonics is modified to take into account dispersion, if it is present.

3.3.2 Introduction of dispersion

In a dispersive media, the sound speed varies with the frequency. As a result, each harmonic travels at its own speed. To introduce dispersion in the program, the speed shift Δc is converted in a phase shift $\Delta\phi$ as follows:

$$\Delta\phi_n = \frac{2*\pi*f_n}{c_0}*\left(1-\frac{c_0}{c_0+n*\Delta c}\right), \tag{3.8}$$

where c_0 is the sound speed of the lowest harmonic which is the difference frequency, f_n and ϕ_n are the frequency and phase of the nth harmonic, respectively. The value of the sound speed shift Δc as a function of the frequency is set previously with the other constants.

Eq. (3.5) can be replaced by

$$v(r,\tau) = \sum_{k=1}^{\infty}\left(\frac{r_0}{r}\right)^a \{G_k^{'}\sin(kw_0\tau) + H_k^{'}\cos(kw_0\tau)\}\exp[-\alpha_k(r-r_0)], \tag{3.9}$$

where $G_k^{'} = G_k*\cos(\Delta\phi_k) + H_k*\sin(\Delta\phi_k)$ and $H_k^{'} = H_k*\cos(\Delta\phi_k) - G_k*\sin(\Delta\phi_k)$.

Therefore, we can see from Eq. (3.9) that if the acoustical parameters of a medium (density, sound speed as a function of frequency, and the nonlinear coefficient) are known, sound propagation through the medium can be characterized. This allows the determination the efficiency of our medium as well as the optimal thickness of the nonlinear layer.

3.4 Layer resonance

In our design, the transducer is composed of a spherical linear projector surrounded by a nonlinear layer. The nonlinear medium is directly in contact with water, as shown in Fig. 3.1. The material has a low sound speed, relative to water, and this difference leads to an impedance mismatch resulting in the reflection of a part of the signal at the material/fluid boundary. The acoustic wave bounces back and forth between the transducer and the water interface. The result is a resonant amplification of the transmitted difference frequency signal. Thus, to predict the source level generated by the projector one must calculate the initial nonlinear propagation and take into account the linear contribution of the thickness resonance of the layer.

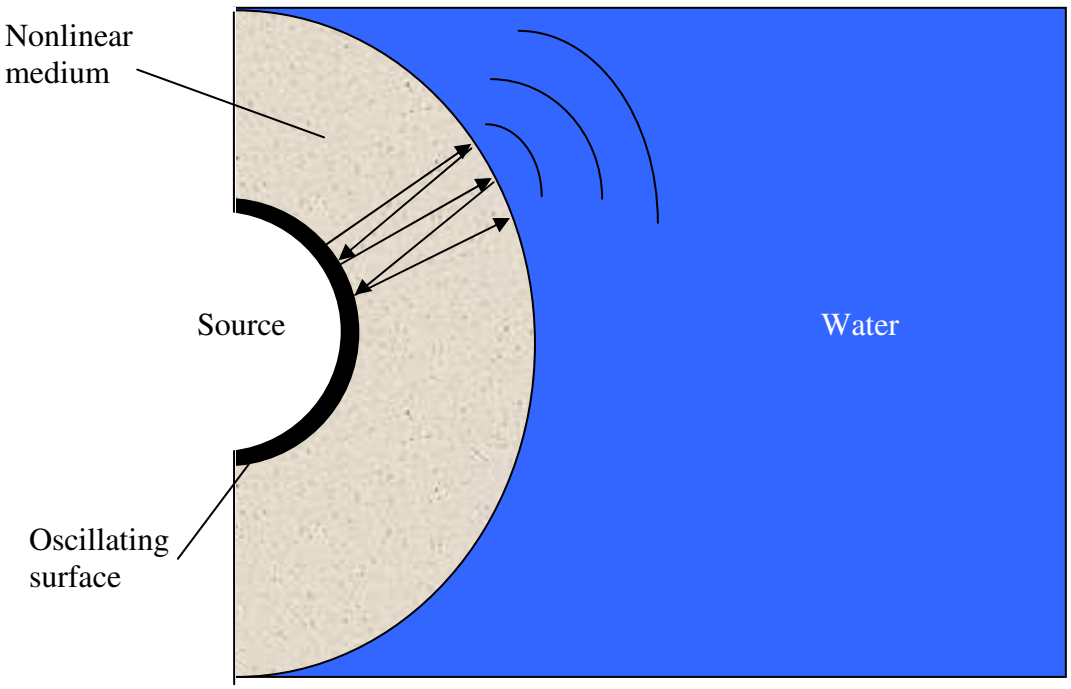

Figure 3.1- Diagram of the layer resonance

The thickness of the layer is determined in order to make the contribution of the primary waves negligible after the first reflection. A linear model can then be used to predict the gain due to the layer resonance. The problem reduces to that of the resonance of a plane wave in a tube with an oscillating piston on one end and a water-layer interface on the other end, as illustrated in Fig. 3.2.

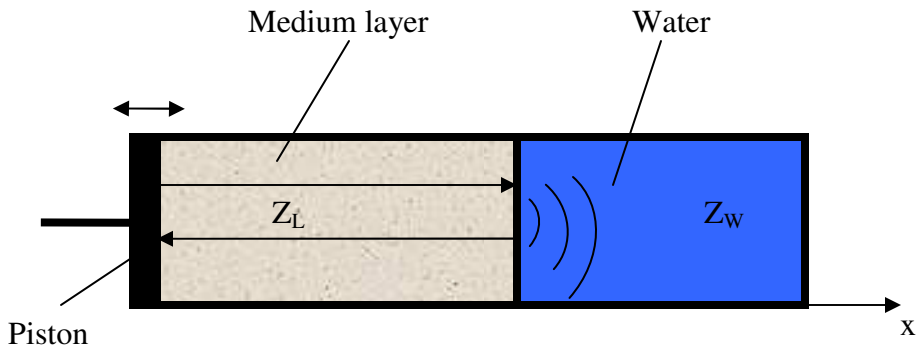

Figure 3.2- Diagram of the simplified layer resonance

The pressure inside the tube has the form,

$$P_T(x) = C_1 * e^{-ik_l x} + C_2 * e^{ik_l x}, \tag{3.10}$$

where k_l is the wave number of the signal in the medium layer. This represents the superposition of a plane wave traveling in the +x direction and a plane wave traveling in the –x direction.

Using Euler's equation, we get the corresponding particle velocity

$$V_T(x) = -\frac{C_1}{Z_L} * e^{-ik_l x} + \frac{C_2}{Z_L} * e^{ik_l x} \tag{3.11}$$

In the fluid, there is only a wave propagating to the right. The infinite extent of the fluid medium eliminates any reflected signal. The pressure is of the form

$$P_W(x) = C_3 * e^{-ik_w x} = C_4 * e^{-ik_w (x-l)}, \tag{3.12}$$

where k_w is the wave number of the signal in water

and the particle velocity

$$V_W(x) = \frac{C_4}{Z_w} * e^{-ik_w (x-l)}. \tag{3.13}$$

The continuity of the acoustic pressure and the particle velocity at the boundary can be written as:

$$P_T(x = l) = P_W(x = l) \tag{3.14}$$

$$V_T(x = l) = V_W(x = l) \tag{3.15}$$

Three pieces of information are required to solve for the three unknown amplitudes. The third one is provided by the boundary condition at the surface of the piston

$$V_T(x = 0) = V_0. \tag{3.16}$$

This gives us the following system of equations:

$$\begin{cases} C_1 * \exp(-jk_m l) + C_2 * \exp(jk_m l) = C_4 \\ \dfrac{C_1}{Z_m} * \exp(-jk_m l) - \dfrac{C_2}{Z_m} * \exp(jk_m l) = \dfrac{C_4}{Z_w} \\ \dfrac{C_1 - C_2}{Z_m} = V_0 \end{cases} \tag{3.17}$$

These equations may be solved for the transmitted amplitude C_4 yielding,

$$C_4 = \frac{Z_m * V_0}{\dfrac{Z_m}{Z_w} * \cos(k_m l) + i \sin(k_m l)}. \tag{3.18}$$

The resonant amplification or gain due to the thickness of the material layer is given by

$$G = 20 * \log_{10}\left(\left|\frac{P(x=l)}{P(x=0)}\right|\right) = 20 * \log_{10}\left(\left|\frac{C_4}{Z_m * V_0}\right|\right)$$

or, (3.19)

$$= 20 * \log_{10}\left(\frac{1}{\sqrt{\left(\dfrac{Z_m}{Z_w} * \cos(k_m l)\right)^2 + \sin^2(k_m l)}}\right)$$

Thus, depending on the properties on the medium (sound speed and density), the frequency and the thickness of the material layer, a gain factor can be computed and introduced into our predictive model.

CHAPTER IV

MEDIUM INVESTIGATION

The theory of the parametric effect has been presented in two previous chapters. In order to optimize the generation of difference frequency of the parametric source, we now examine the various components of the nonlinear layer.

4.1 Desired properties of the medium

Our goal is to design a medium with a large nonlinear parameter over an extended range of static pressure, i.e., water depths.

The nonlinear coefficient is defined by:

$$\beta = 1 + \frac{B}{2A} = 1 + \rho_0 c_0 \left(\frac{\partial c}{\partial p} \right)_{s,\rho=\rho_0} \tag{4.1}$$

Large values of this coefficient can be obtained by designing a medium whose sound speed varies strongly with hydrostatic pressure. Microspheres are used in order to create such a medium [23, 24, and 25]. At low hydrostatic pressure, microspheres appear hard due to their hoop stiffness. As the pressure increase, microspheres start to buckle and get

the shape of an oblate spheroid which makes them very compliant. This compliance allows the deformation of the microspheres when a sound wave propagates through the medium. The compression part of the wave makes them buckle even more whereas the depression part makes them release. Nonlinearity of the medium is explained by this phenomenon. Previous studies [23, 24] showed that the deformation of the microsphere of the bubbles is fast enough to react to sound waves. Thus, static measurements can be realized to predict the medium effectiveness. The sound speed is also modified by the change of compliance of the medium according to

$$c = \sqrt{\frac{K_b}{\rho_0}}, \tag{4.2}$$

where K_b is the static bulk modulus. This modulus is defined as

$$\frac{1}{K_b} = -\frac{1}{V_0}\frac{dV}{dP}. \tag{4.3}$$

Equations (4.1), (4.2) and (4.3) show us that the sound speed and the nonlinear coefficient of the medium can be determined by measuring the change of volume as a function of the change of pressure.

Our medium is composed of a mixture of microspheres and plastic rubber, the latter constituting the matrix.

The parameters that will be investigated in the optimization process are:

- Size of the micropheres

The microspheres that we use are made by Expancel®. They consist of a gas encapsulated by a polymer shell. Our interest in the microspheres concerned their buckling properties. The buckling pressure is given by [21]

$$P_{cr} = \frac{2E_s t^2}{r^2 \sqrt{3(1-\sigma_s^2)}}, \qquad (4.4)$$

where σ_s is the shell's Poisson's ratio of the shell, E_s is the Young's modulus for the material of the sphere, r is the radius and t is the thickness.

We are looking for microspheres that buckle at a pressure as high as possible. We will, therefore, tend to minimize the radius and to maximize the thickness. Different kinds and sizes of microspheres are available. Properties of the different types are given in appendix (Appendix II).

- Hardness of the matrix

The matrix has to be soft enough to allow microspheres to buckle and to keep their compliance. The source also has to be easy to handle and robust enough to keep its shape underwater. The matrix cannot be a liquid because of risks of leaking.

- Microphere ratio

This ratio has a great effect on the sound speed and therefore on the nonlinear coefficient. Indeed, a large volume fraction of microspheres in the medium will lead to a very compliant medium and, at the same time, to low density. The result is a very low sound speed (even lower than the air sound speed) that, combined with a large nonlinear parameter, can yield to a large parametric effect.

- Layer thickness

The determination of the previous parameters sets the characteristics of the medium. This allows us to run the simulation program presented in the previous chapter. The result of the simulation will then provide us with an indication of the thickness needed in order to obtain the best transfer of energy from the primaries to the difference frequency signal. Thickness will also be an important parameter for the resonance layer effect. A thin layer will reduce the absorption and scattering phenomena.

4.2 Static measurements

Static measurements are performed to obtain the bulk modulus of the composite medium. A system composed of a pressure vessel coupled to a calibrated pump and a pressure meter is used to measure the volume change as a function of hydrostatic pressure, as illustrated schematically in Fig. 4.1. The vessel is made of stainless steel and has a capacity of 216 cm^3. The pump allows one to control the change of volume in a calibrated manner. Samples, one at a time, are introduced into the vessel which, is then filled up with castor oil. The same oil is used in the pump. A vacuum is then pulled on the whole system to remove air which introduces an undesired additional compliance. The presence of air bubbles can easily be detected by analyzing the initial measurements above ambient pressure. Free air bubbles significantly increase the compliance; however, they collapse quickly resulting in a significant decrease in compliance. Thus, the initial behavior provides immediate information on the presence of air indicating a valid measurement set-up or the need for further evacuation.

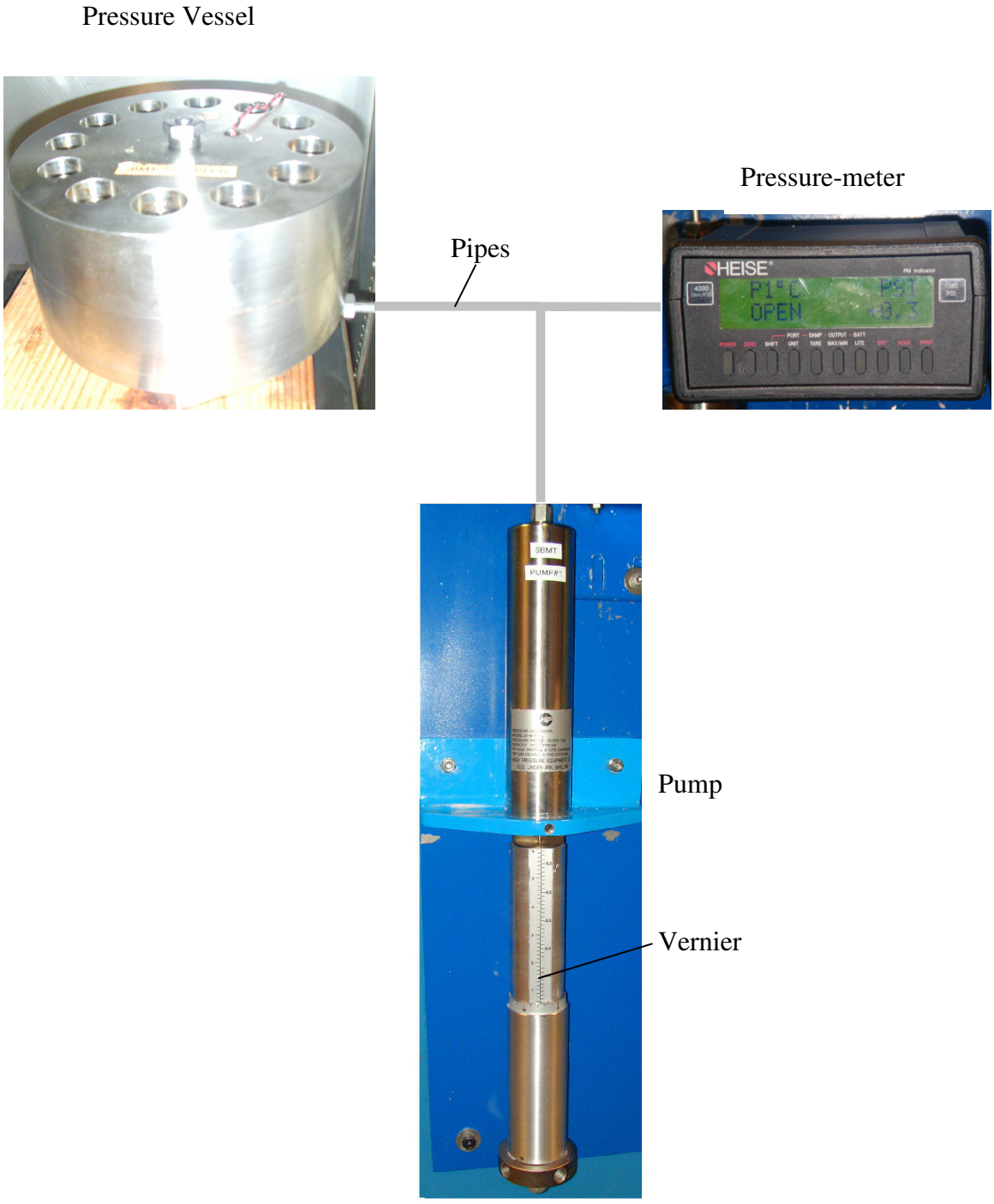

Figure 4.1- Static measurement equipment

The total variation of volume, with increasing hydrostatic pressure, is given by

$$\Delta V_{total} = \Delta V_{sample} + \Delta V_{oil} + \Delta V_{vessel} . \quad (4.5)$$

ΔV_{total} corresponds to the measured variation of volume, and ΔV_{sample} is the value of interest. Thus, ΔV_{oil} and ΔV_{vessel}, the expansion of the entire device (vessel+pump+pipes) must be determined from prior measurements.

The bulk modulus of castor oil is known (K_{oil}= $2.17*10^9$ Pa) [21] and gives us ΔV_{oil}. Then, the compliance of the vessel is measured by filling it with water only and measuring the change of volume as a function of the change of pressure. Water is used because its properties are well known and of its high bulk modulus. The total volume change reduces to

$$\Delta V_{total} = \Delta V_{water} + \Delta V_{vessel} . \quad (4.6)$$

As ΔV_{total} and ΔV_{water} are known, ΔV_{vessel} can be deduced by the determination of the total variation of volume when the vessel and the pump are filled up with water. (See Fig. 4.2)

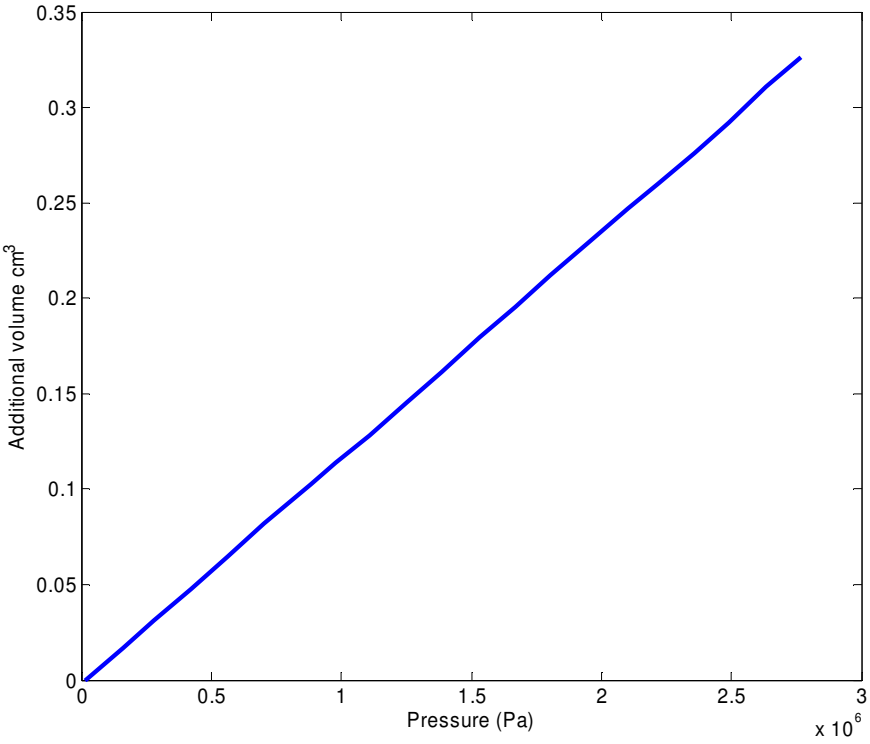

Figure 4.2 Variation of volume as a function of the pressure of a vessel filled up with pure water

Measurements yielded

$$\frac{\Delta V_{vessel}}{\Delta P} = \frac{\Delta V_{total} - \Delta V_{water}}{\Delta P} = 1.5 * 10^{-8}\ cm^3/Pa = 1.5 * 10^{-11}\ m^5/N \qquad (4.7)$$

Different samples can then be tested.

A typical type of curve obtained from such measurement is given in Fig. 4.3

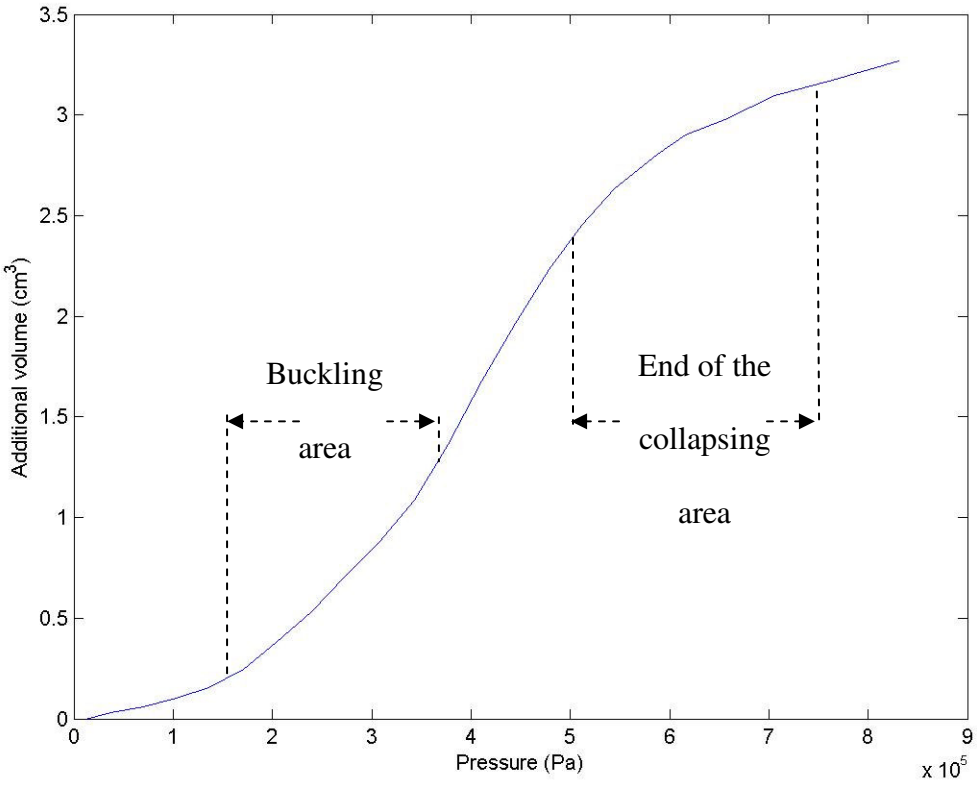

Figure 4.3- Example of plot of the variation of volume in function of the variation of pressure of a mixture of microspheres and castor oil

We can distinguish several zones. At low pressure, microspheres appear to be stiff due to the hoop stiffness of a sphere. Above approximately 150 kPa, the pressure is high enough for the large diameter and thin walled microsphere to buckle. From this point, the compliance, the slope of the curve, increase reaching a maximum when all the microspheres are buckled. With further increase in hydrostatic pressure, the microspheres begin collapsing. There is a non-uniform microsphere size distribution, and the smallest micropheres start buckling while the largest ones have already collapsed. Once the smallest collapse, the medium becomes stiff again and the bulk modulus of the composite

medium is then equivalent to that of the matrix material. The process is reversible. Once the pressure is released, the microspheres return to the initial spherical shape.

The buckling and collapsing regions are characterized by the rapid change in the slope of the compliance and are the regions where the nonlinear coefficient is the largest. They are therefore the primary regions of interest. Note also that the main difference between the two regions is the direction of curvature. In the buckling region, the slope is increasing along with pressure; therefore the bulk modulus (Eq. 4.3) and the sound speed (Eq. 4.2) are decreasing which yield a negative nonlinear coefficient (Eq. 4.1). In the collapsing region, this is the opposite, the slope is decreasing when the pressure gets higher, and therefore, the nonlinear coefficient of the corresponding range of pressure is positive. This opposite signs for the nonlinear coefficient result in a waveform which will be distorted either as a rarefactive (buckling part) or a compressive (collapsing part) shockwave. The plot also indicates that the region between the buckling and collapsing region has a nearly constant slope. In this region, the sound speed of the composite medium does not vary significantly with hydrostatic pressure and, thus, the coefficient of nonlinearity will be low.

4.3 Parameters values

The different measurement results led to the following parameters values:

- Among the Expancel® product range, two types of micropheres present small size and high density: The 461 DE 20 d 70 and the 551 DE 20 d60 model. To decide between both, measurements and simulations are realized to predict their performances. As explained previously, measurements of the variation of volume as a function of the variation of pressure allow us to approximate sound speed and nonlinear coefficient of the medium. These parameters are introduced in the simulation program presented in section 3.3. The other inputs (amplitude of the particle velocity of the primaries and propagation distance) are arbitrarily chosen based on previous work [25] and are the same in both cases. In these measurements, microspheres are mixed with castor oil, the propagation distance is 2cm and the particle velocity corresponds to a driving voltage of 180V for each primaries. The simulation gives us the particle velocity of the difference frequency after propagation. The sound pressure level (SPL) at 1m is then deduced thanks to the formula

$$SPL_{1m} = 20\log\left(\frac{P_{@1m}}{P_{ref}}\right), \tag{4.8}$$

where P_{ref} is the reference pressure and is equal to 10^{-6} Pa.

The pressure P is linked to the particle velocity by

$$P_{@1m} = \frac{r_0}{R} P_s = \frac{1}{R} * \frac{G_{res} * v * \rho * c * r_0}{\sqrt{1 - \frac{1}{k^2 r^2}}}, \qquad (4.9)$$

where r_0 is the external radius of the sphere, R=1m, P_s is the pressure at the surface of the transducer and G_{res} is the gain due to the resonance layer.

Results are presented in Fig. 4.4

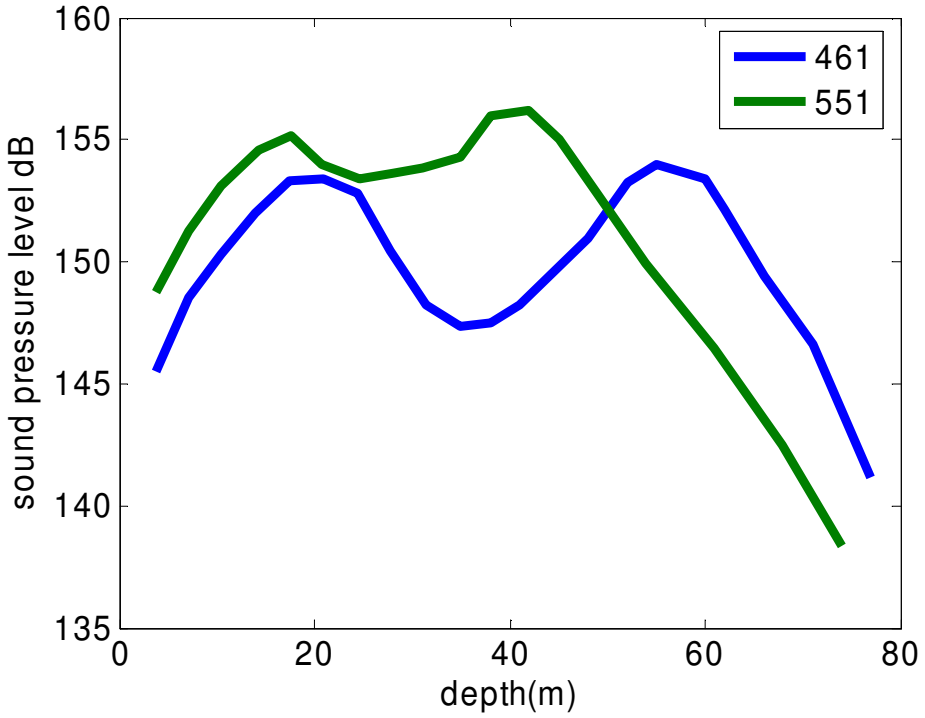

Figure 4.4 Comparison of the performances of 2 kinds of microspheres

Both models present similar performances at low depth but the 461 model present better results for depths above 50m of depth. Therefore, the micropheres model 461 DE 20 d 70 were chosen.

- For the matrix, in order to match all the requirements, urethane seemed to be the best choice because of its flexibility, its softness and its easy use.

  To allow microspheres to behave, and therefore, to buckle as freely as possible under pressure we need a very compliant matrix. Thus, investigation was made to find a very soft urethane. The softest samples that we were able to find had a hardness of 15A. Polyurethanes are composed of two parts that have to be mixed together; one of the parts is the catalyst. Even if the total curing time is usually pretty long (with an optional oven curing part), the mixture tends to become very viscous fairly rapidly especially in the presence of microspheres. This makes pumping delicate. The tested polyurethane was the F-15 made by BJB Enterprises, Inc (properties are described in appendix III). Its simulated performances are presented in Fig 4.5

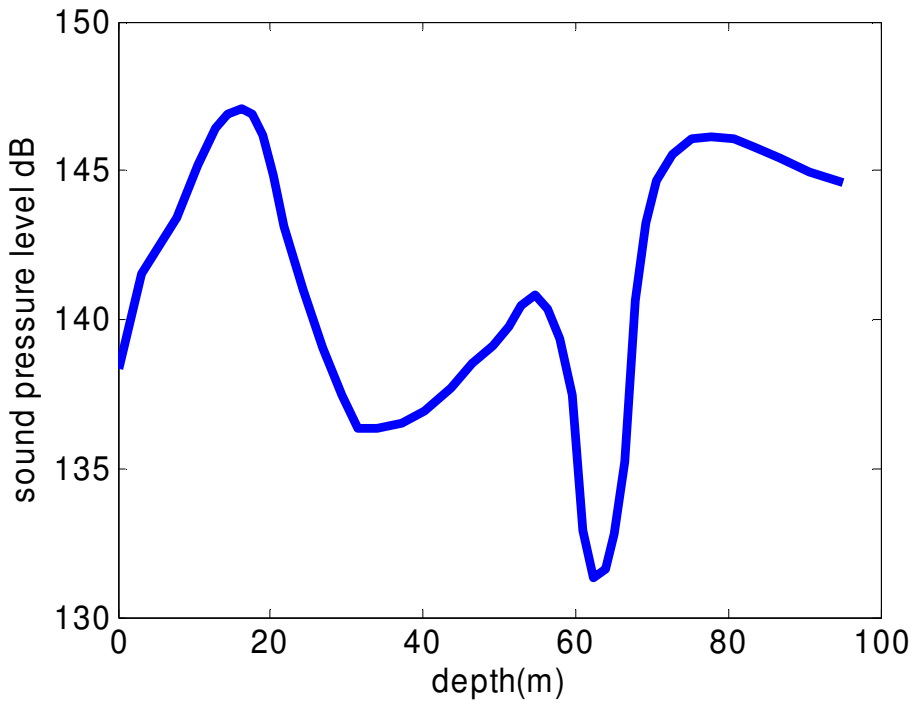

Figure 4.5 Predicted performance of the medium composed a F-15 urethane rubber and a void fraction of microspheres of 20%

We can observe that the curve has the same characteristics that the one where microspheres are mixed with oil (Fig 4.4). We can observe the two regions with high SPL that corresponds to the buckling and the end of the collapsing range of pressure as well as a drop of the efficiency in between. This means that this rubber does not prevent micropheres from buckling. Therefore, it can be used as a matrix of our composite medium.

- To determine the optimal ratio of microspheres in the medium, measurements were performed with three different void fractions. After simulation, the following results are obtained (Fig. 4.6)

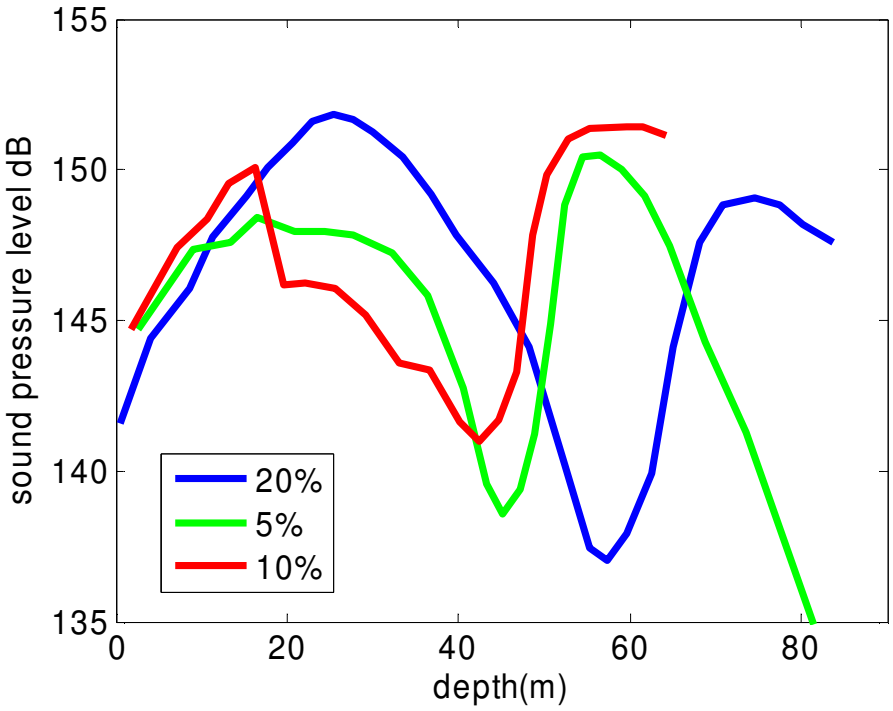

Figure 4.6- Comparison of the efficiency with different void fractions

On the plot, we can see that the curve corresponding to the 20% microsphere fraction produces higher SPL in the range of 20-30m of depth and that the drop of efficiency occurs at higher depth. On the basis of these results, the 20% fraction was chosen.

- All the previous parameters determine the properties of the medium. We now have enough tools at hand to estimate the sound speed and nonlinear

coefficient of the medium. These parameters can then be used as inputs in the program presented in the previous chapter. Results of the simulation, that is to say, the amplitude of the difference frequency as a function of the propagation distance presented on Fig 4.7, allow us to determine the appropriate thickness of the layer.

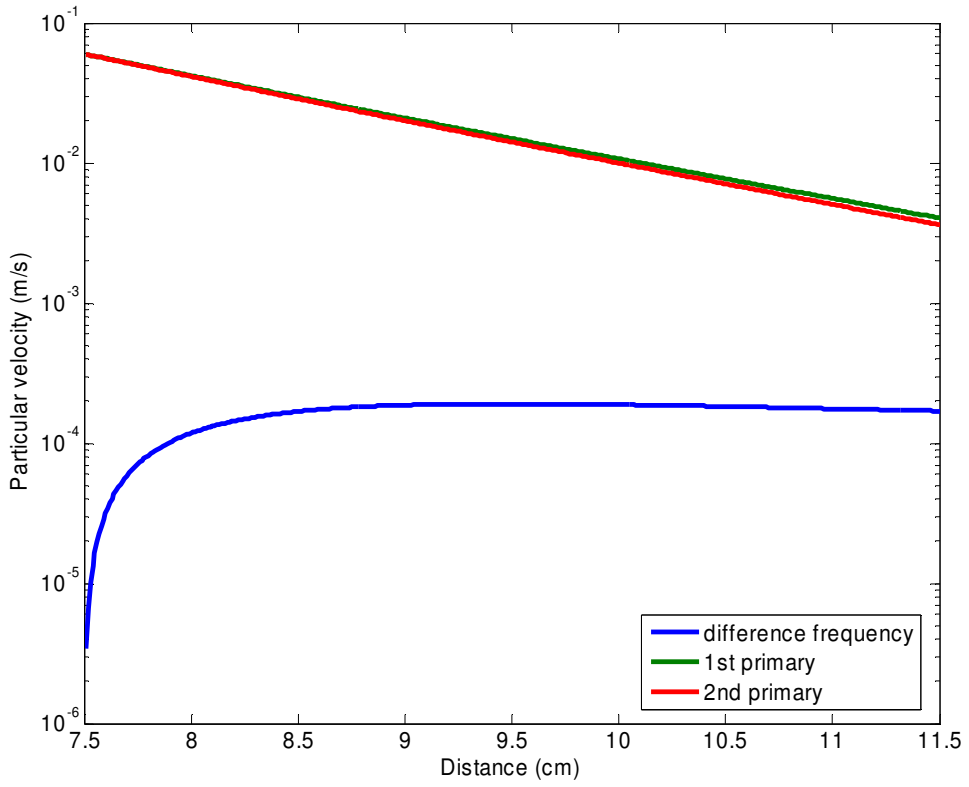

Figure 4.7 Evolution of the amplitude of the difference frequency in function of the propagation distance

On the previous plot, one can see that the amplitude of the difference frequency grows fast in the first centimeter but is not growing anymore after 2cm which is our chosen thickness. After 2cm the transfer of energy is not able to compensate for spherical spreading and losses anymore.

CHAPTER V

SOURCE CONSTRUCTION

This chapter details the practical assembly of the parametric source, which consists of a spherical transducer surrounded by a nonlinear medium layer.

5.1 Linear transducer

The transducer referred to by the manufacturer as USRD F56 PZT-IV is a 7.5cm outer radius sphere made of 2 piezoelectric hemispherical shells adhered together. The shells are covered on both sides with a thin silver layer which acts as an electrode. The outer silver layer was damaged during a previous experiment, and a new one was applied. To choose between the different silver paints available, conductivity and sticking strength are tested. It has to be noted, that not only does the paint have to adhere to the ceramics, but also the protective paint and the urethane rubber have to stick to the silver paint. The Leitsilber 200 model made by Ted Pella, Inc matched with all the requirements and was therefore chosen. The ceramic sphere was first cleaned up with turpentine to remove any greasy agent that would prevent adhesion of the paint. After painting, the capacitance of the source in function of the frequency was measured to check the quality of the new electrode.

The voltage is applied through two electrical cables soldered on the silver of the inner and outer side of the shell as shown in Fig 5.1 and the external surface of the source is painted to protect the silver layer.

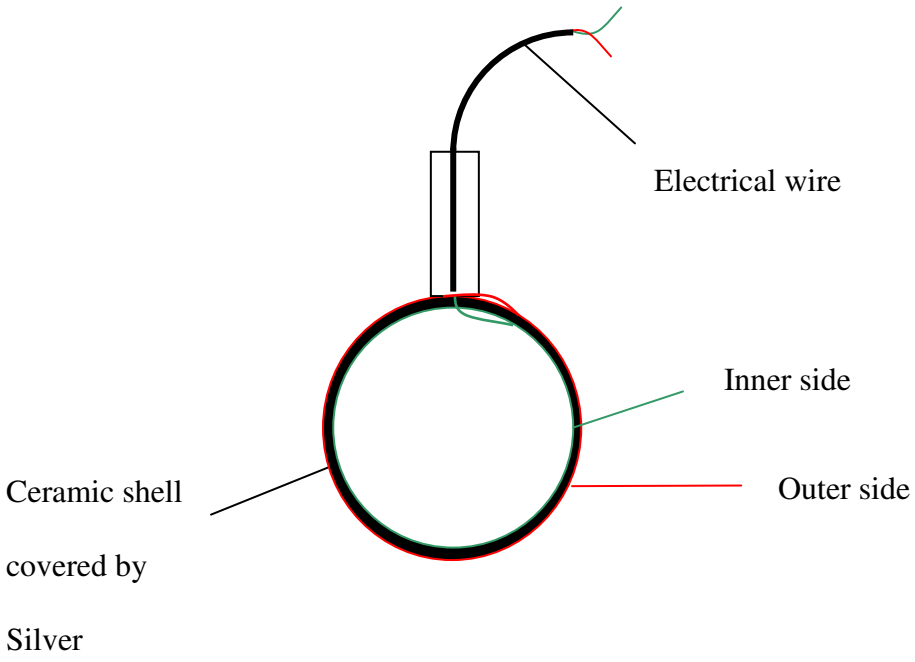

Figure 5.1 - Diagram of the omnidirectional piezoelectric transducer

5.2 Layer Design

To create the 2cm layer around the source, two different ways were tested. The first approach was to make a mold all around the spherical source, pour the medium in it and then pull a vacuum on the entire system to remove bubbles created by pouring the medium. The main issue with this procedure was the high viscosity of the medium which made it difficult to remove the bubbles. Pumping makes air bubbles expand but, if the medium is too viscous, they do not burst and large air cavities remain in the medium.

The other approach consisted in making tiles and gluing them to the source. As the volume of medium needed to make one tile is fairly small, vacuum can be pulled fast enough to overcome the viscosity issue. In order to fit the shape of the sphere, a soccer ball geometry also called truncated icosahedron was chosen. It is a 32 face polyhedron composed of 20 hexagons and 12 pentagons (See Fig.5.2)

Figure 5.2- Geometry of the truncated icosahedron

In order to make the overall shape spherical, lower and upper faces of the polygons had to be curved (See Fig 5.3).

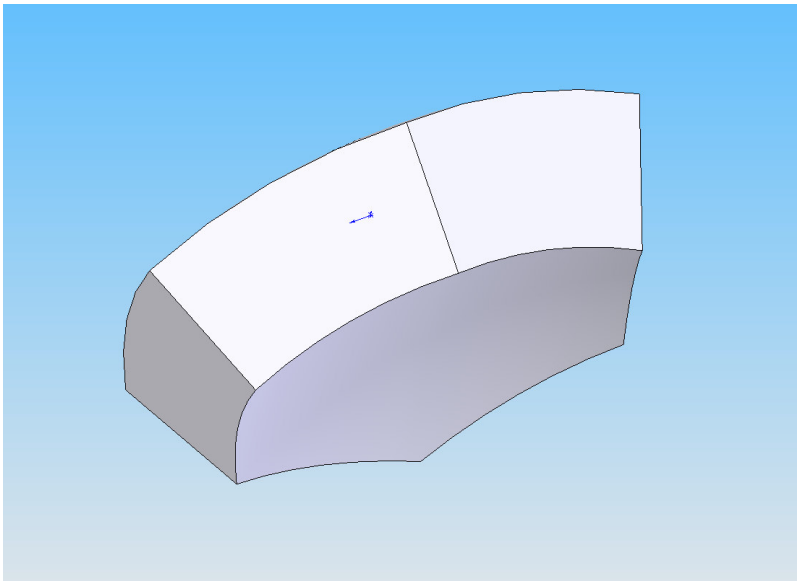

Figure 5.3- 3D drawing of a tile

Technical drawings of the tile shapes are available in appendix (appendix IV).

To fabricate these tiles, molds were created using Plexiglas. An example is shown n Fig. 5.4. Curved surfaces were obtained by heating the Plexiglas to make it soft and malleable, and then, by bending them on a sphere of the desired radius. To prevent the mixture from sticking to the mold, a polyvinyl alcohol (PVA) mold release made by Craft Resins® was used.

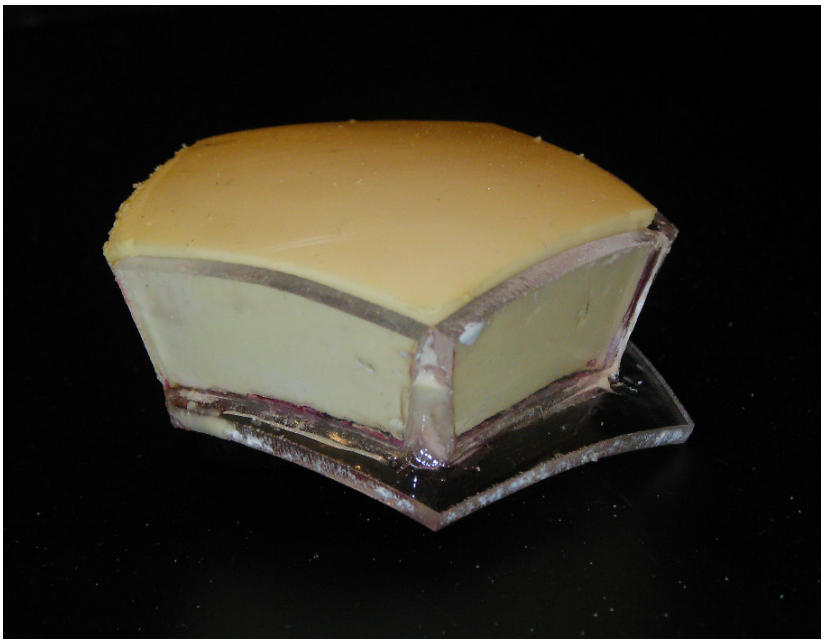

Figure 5.4- Plexiglas mold and tile

5.3 Assembly

In order to attach the tiles to the transducer, the proper adhesive had to be used: it had to be strong enough to withstand hydrostatic pressure, and it had to present a good acoustic impedance match to the tile material in order to minimize interface losses. The F-15 polyurethane combined these two criteria and was used to glue the tiles.

After mixing of the 2 parts, bubbles were removed from the polyurethane mixture by placing it in a vacuum for a few minutes. An intermediate stage of the transducer assembly is shown in Fig. 5.5.

Figure 5.5- Nonlinear layer assembly

After assembly, the capacitance of the source was measured again to make sure that the source was not damaged. This also told us the value of the resonance frequency. This value is important in order to determine the frequencies of the 2 primaries and is equal to 12.7 kHz.

CHAPTER VI

TANK MEASUREMENTS AND RESULTS

Measurements have been performed in the acoustic tank facility in the Love building of the Georgia Institute of Technology. The tank is approximately 6m deep, 8m wide and 12m long; the depth restricts the range of achievable hydrostatic pressures.

6.1 Settings

6.1.1 Driving voltage

An arbitrary waveform function generator (Polynomial waveform synthesizer Analogic® model 2020) was used to generate the desired input signal to the power amplifier.

The signal had the following form:

$$V(t) = A * \sin(F1 * t + 0.5) + B * \sin(F2 * t), \tag{6.1}$$

where $F1$ and $F2$ are the primary frequencies. These frequencies are chosen to be close to the resonance frequency of the transducer, 12.7 kHz, in order to obtain the maximum velocity from the spherical projector. They can be modified as desired to obtain any set of difference frequencies.

A and B are arbitrary coefficients to adjust the desired amplitude of the signal. They are normally equal as both primaries need to have the same amplitude for the maximum efficiency.

The first sine was slightly time shifted to prevent the presence of a high slope at the start of the signal introducing a transient response of the amplifier. The generated signal was sent to a kilowatt amplifier made by Instruments, Inc (model L6) and then transmitted to the source. If one attempts to drive the amplifier with too large of an input signal, nonlinearities can be created by the amplifier itself. The potential for the generation of these nonlinearities has been studied by analyzing the signal generated by the amplifier, and it was concluded that they were negligible if the amplifier was used within its normal range (The warning lights for the voltage and current limits not indicating an overdrive condition). The amplitude of the signal sent to the source was measured using the voltage monitoring output of the amplifier which gives 1% of the actual output signal. The duration of the signal was arbitrarily taken to be 10ms. Since we wanted to study low frequency sound waves, it cannot be much smaller in order to measure at least one period of the signal of interest.

6.1.2 Data acquisition

The hydrophone used in the experiment was a model 8100 manufactured by Brüel & Kjær Sound & Vibration (calibration chart available in appendix V). To position the hydrophone 1m away from the center of the source, a plastic tube, perforated to prevent the trapping of air, was used. The transducer was attached to a metal cable. Marks were put on the cable to monitor the depth of the source.

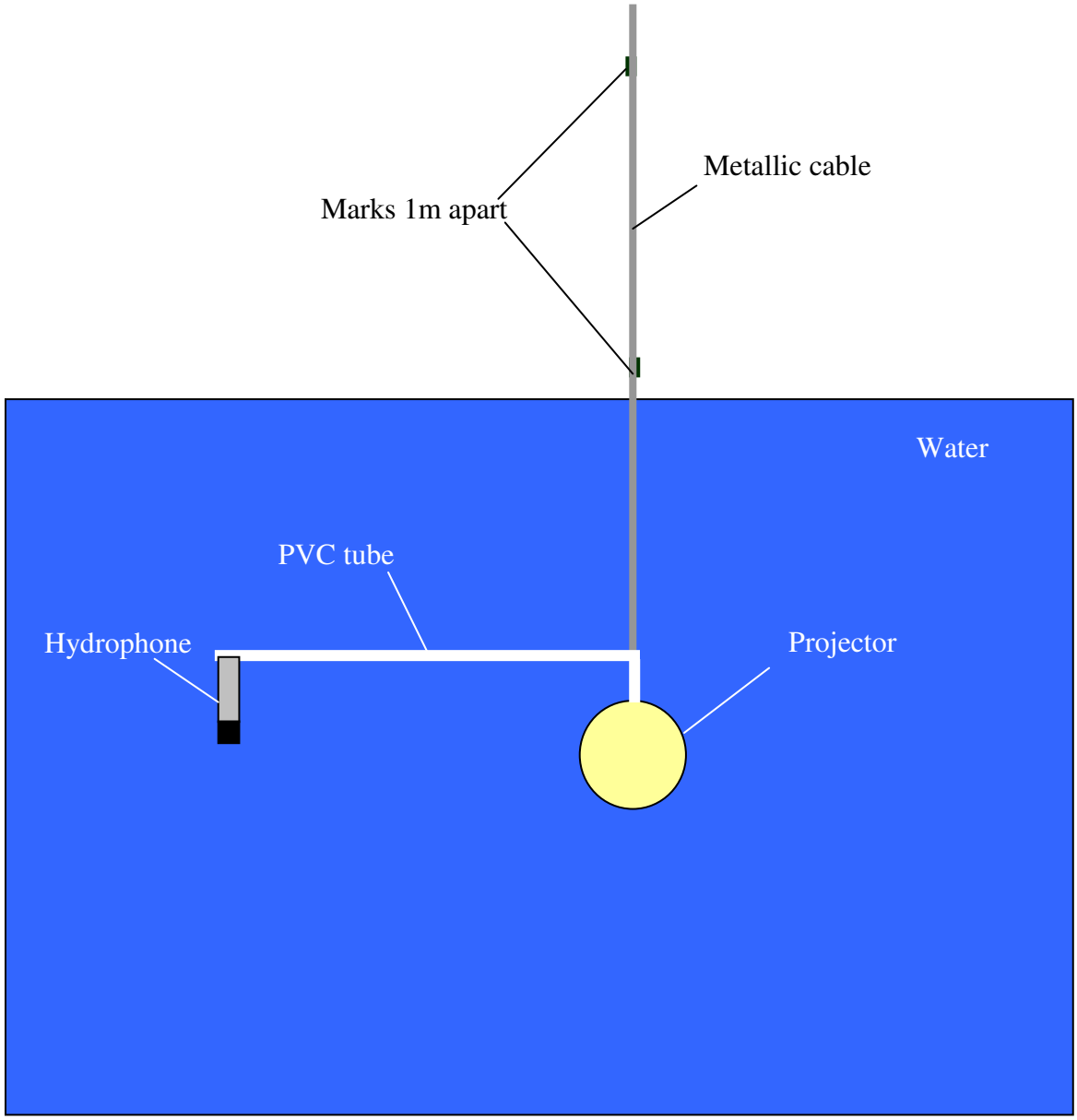

Figure 6.1- Diagram of the source during tank measurement

As the dimensions of the tank are relatively small, attention must be paid to surface reflections. Reflections can occur at the bottom, at the four side walls and also at the top, at the interface air-water. One way to avoid reflected signals is to simply time-gate them

out of the response. That is, use only that portion of the received signal prior to the arrival of the first reflection. The corresponding time can be found by dividing the travel distance of the reflected wave by the speed of sound in water (approximately 1480 m/s). The problem with this approach is that it limits the lowest frequency that can be measured.

The acoustic pressure, converted by the hydrophone into an electrical signal, was digitally recorded. This signal included all the frequencies, and the data had therefore to be processed and filtered to obtain the signal of interest which is the difference frequency signal.

6.1.3 Data processing

To convert the measured signal (in Volt) into pressure (in Pascal), we used the sensitivity of the hydrophone given by the manufacturer's calibration $(\sigma = 51.3\mu V / Pa)$. Filtering was performed in Matlab®. An elliptic band pass filter was used. The small size of the frequency band combined with the large sampling frequency made the design of the filter somewhat difficult. Indeed, parameters (order and cut-off frequency band) have to be well chosen to obtain a stable filter. To check the validity of the filtered signal, a Fourier transform was also performed to check the presence and the amplitude of a peak at the difference frequency. The equation of the filter is given by:

$$Y(z) = \frac{0.0005 - 0.0019z^{-1} + 0.0023z^{-2} + 0.0019z^{-4} - 0.0005z^{-5}}{1 - 5.9983z^{-1} + 14.9916z^{-2} - 19.9839z^{-3} + 14.9844z^{-4} - 5.9925z^{-5} + 0.9986z^{-6}} X(z) \tag{6.2}$$

And is represented on Fig. 6.2.

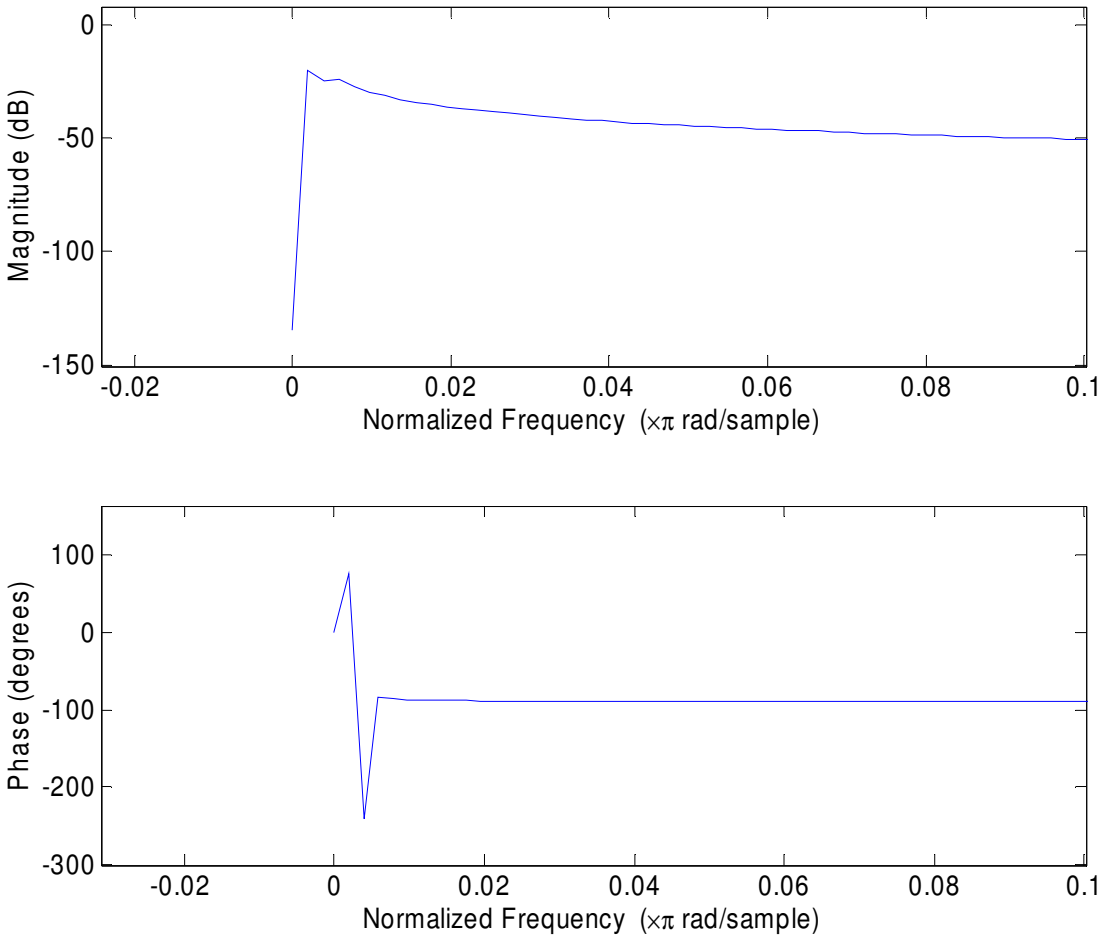

Figure 6.2- Plot of the magnitude and the phase of the filter as a function of the frequency

6.2 Tank measurements

The first experiment was performed with primary frequencies at 12.9 and 13.2 kHz (we also tested with 12.5 and 12.8 kHz), which are close to the resonance frequency of the source; this produced a different frequency of 300 Hz. The waveform used also corresponded to that used by Dumortier [25] during his measurements and would have allowed us to compare both results. Measurements were performed at a 2m depth. Unfortunately, no energy was detected at the difference frequency; the measured value corresponds to the noise level and no peak can be observed on the Fourier transform. This implies that the efficiency of our source is very low in such conditions. Two explanations are possible, either our source is not efficient at all or a higher hydrostatic pressure is required. The idea was then to increase the difference frequency value which would improve the efficiency of the energy transfer as the difference frequency signal is proportional to the frequency (Eq. 3.18 and 3.19). Difference frequencies of 500, 800Hz and 1 kHz were tested but the signal at 500 and 800Hz were very low so that the new difference frequency was set at 1 kHz and obtained with a driving signal whose components were 11.9 and 12.9 kHz (See Fig 6.3).

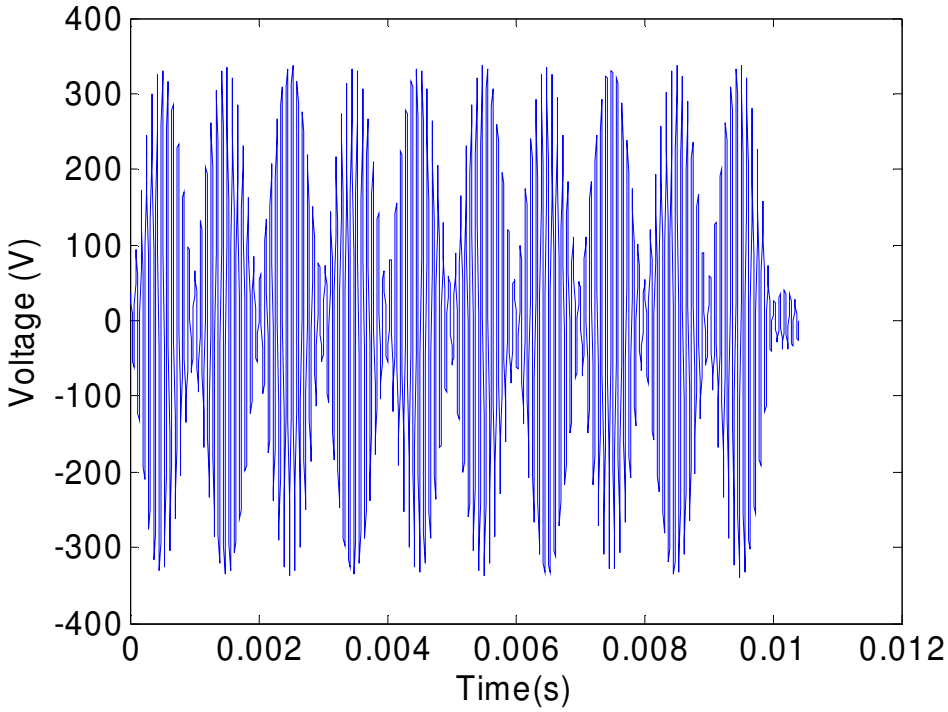

Figure 6.3- Driving voltage signal created by the function generator and amplified

After amplification, the signal applied to the source had an amplitude of approximately 160V for each primary. The measured waveform, at a distance of 1m, obtained with the drive signal in Fig. 6.3 is plotted in Fig.6.4.

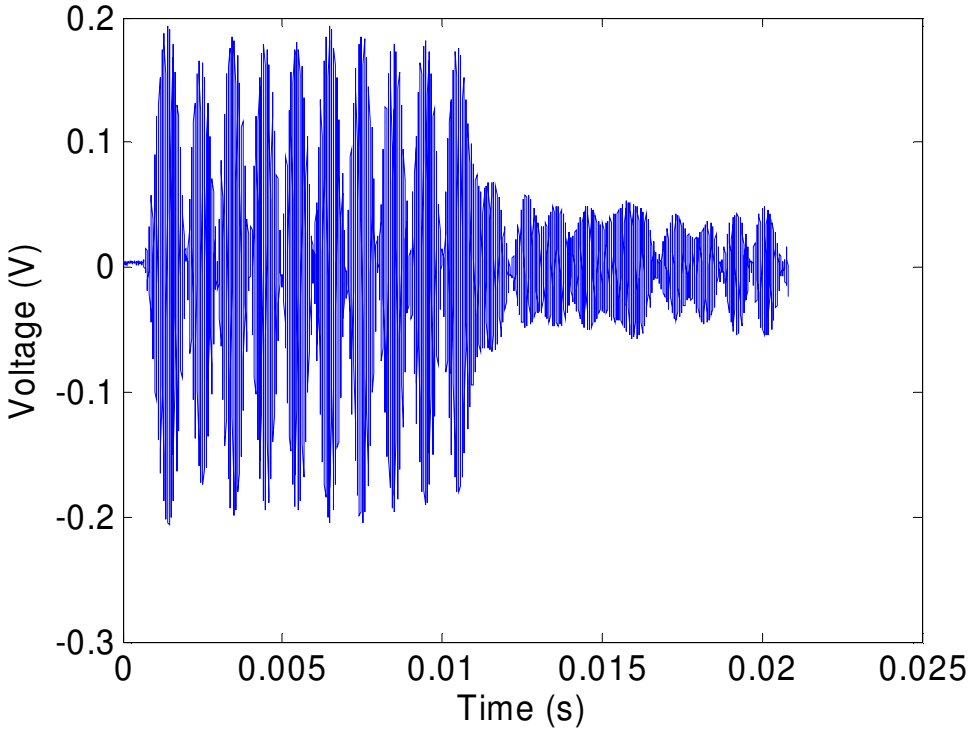

Figure 6.4- Signal measured by the hydrophone at 1 m away from the source

The signal displayed on Fig 6.4 is not filtered and is therefore contained both primaries, as well as their harmonics, the sum, and the difference frequency. Note the arrivals after 10 ms, indicating the presence of boundary reflections. The signal was then filtered to keep the 1 kHz component only (see Fig. 6.5).

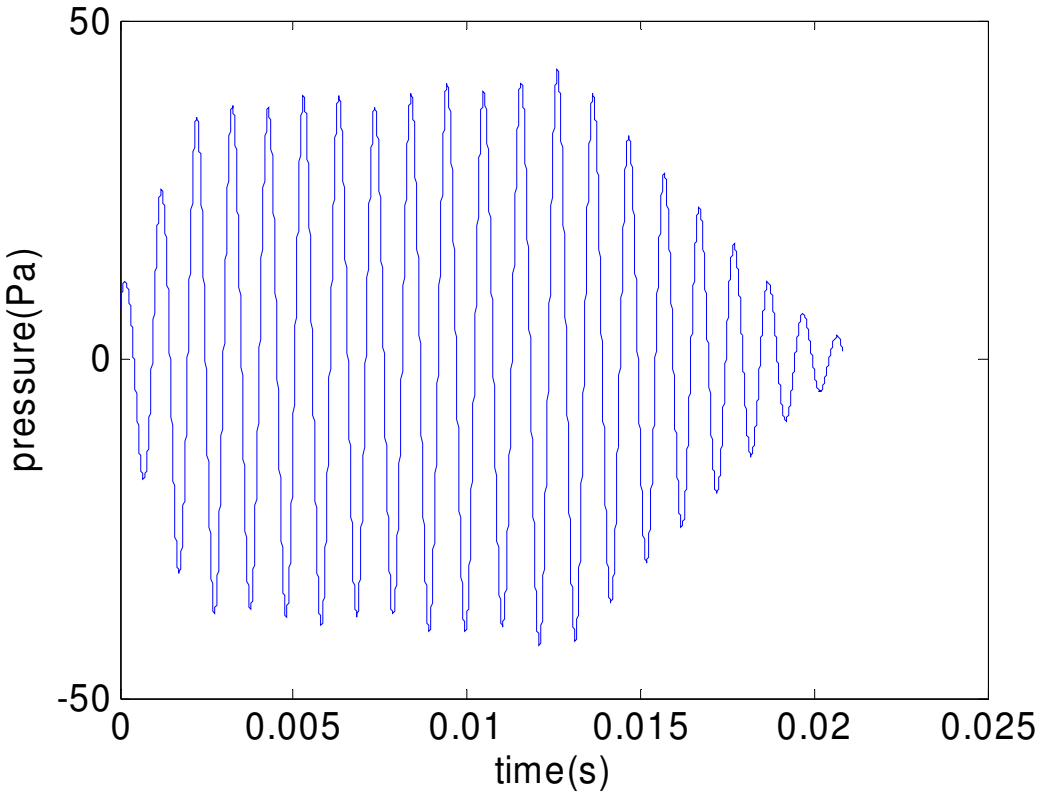

Figure 6.5- The waveform in Fig. 6.4 after low-pass filtering to yield the difference-frequency component at 1 kHz

The hydrophone was positioned 1m away from the source which was 2m deep so that the travel distance for the first reflection wave was 4.12m. This corresponds to 2.8 ms of travel time considering a sound speed in water of 1450 m/s. The amplitude then had to be determined at a time prior to 2.8 ms. Doing that results in an amplitude of 37.3 Pa regarding the previous plot. The sound pressure level at 1m is given by

$$SPL = 20 * \log\left(\frac{P}{P_{ref}}\right) = 151 dB\,, \tag{6.3}$$

where P is the acoustic pressure in Pa and P_{ref} is the underwater reference pressure (1µPa).

This value needed to be compared with the result that would be obtained by driving the source linearly. To do that, we use the typical TVR (Appendix VI). At 1 kHz, the given value is 108 dB/V ref. 1µPa which would yield a sound pressure level of 158 dB. The simulation gave a predicted value of 154.5 dB. Our result appears to be 7 dB lower than the linear source driven at the same frequency and 3.5 dB lower than the simulated value. According to the theory, the efficiency of our projector was supposed to increase with depth as the microspheres buckle. We then needed to carry out measurement at a higher hydrostatic pressure. We also had to find a way to explain the low efficiency of the source. The first idea was to perform other measurements in the tank at different depths. The amplitude of the difference frequency obtained for a range of 3 to 4m depth was lower than the value at 2m, which contradicts theoretical predictions and which would mean that there is an unknown nonlinear effect at very low static pressure. The plot of the sound pressure level as a function of the depth is given in Fig.6.6. On this graph, we observe that the anomalous behavior of increased performance extends to 0.5m depth.

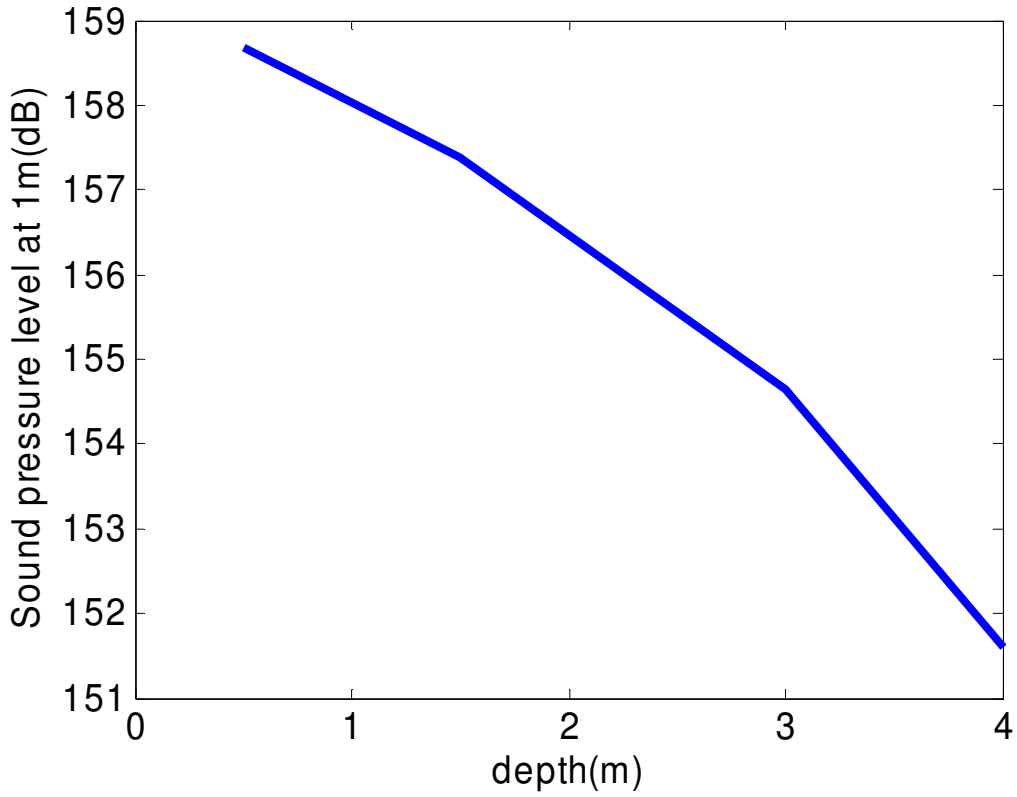

Figure 6.6- Sound pressure level measured in the water tank as a function of the depth with a difference-frequency component at 1 kHz

However, the limited depth of the tank prevented us from going up to a hydrostatic pressure of 20 PSI (or 14m deep) which corresponds to the predicted buckling pressure of the microspheres. In order to overcome this issue, we decided to place the source inside a pressure chamber and to take it to higher static pressure, in air.

6.3 Pressure chamber measurements

To perform these measurements, a pressure tank equipped with a manometer and made by Binks® was used. The entire system is shown in Fig. 6.7. Pressure was created by an electric pump made by Id Interdynamics.

Figure 6.7- Picture of the pressure chamber

The velocity of the projector surface was measured with accelerometers. These were chosen to be as small as possible to prevent them from perturbing the vibrations of the surface and biasing the measurements. The accelerometers used were made by PCB Piezotronics, Inc. (Model 352B22). The other advantage of this configuration was that these were local measurements. Accelerometers were stuck on one tile (at the center, to avoid any side effect as depicted on Fig. 6.8) so that the response of the accelerometer to the sound related the behavior of this particular tile. This allowed us to compare the behavior of the different tiles.

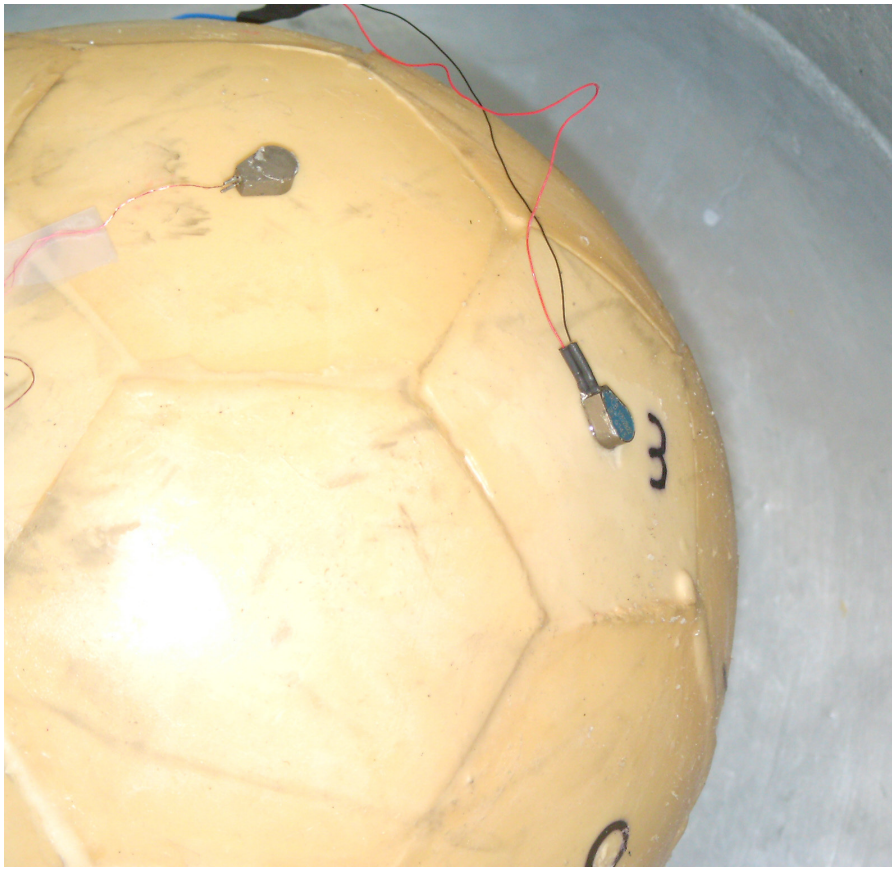

Figure 6.8- Picture of the accelerometers stuck on the source

In this case, the contribution of the layer resonance has to be recalculated. Indeed, in this configuration, the interface medium-air creates a pressure release termination (Fig.6.9).

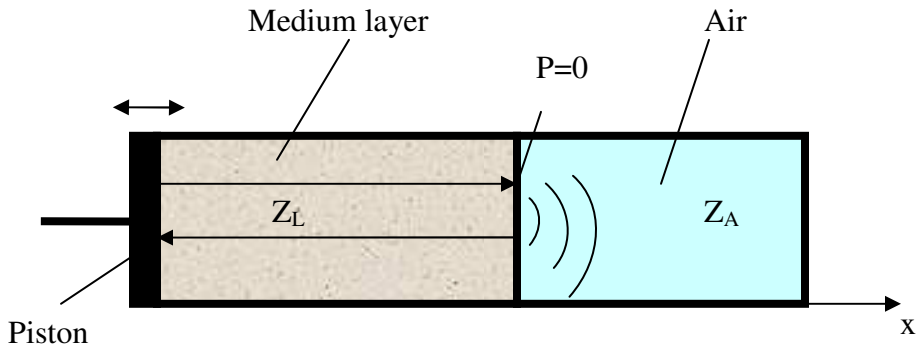

Figure 6.9- Diagram of the simplified layer resonance in air

The pressure inside the tube is defined as

$$P = P^{-}e^{-ik_l x} + P^{+}e^{ik_l x} \tag{6.3}$$

The pressure at the interface is set to 0 which gives us at $x = l$

$$P(x = l) = P^{-}e^{-ik_l l} + P^{+}e^{ik_l l} = 0 \tag{6.4}$$

Which gives

$$P^{+} = -P^{-}e^{-2ik_l l} \tag{6.5}$$

In term of the velocity, we have:

$$V_T(x) = -\frac{P^{-}}{Z_m} * e^{ik_l x} + \frac{P^{+}}{Z_m} * e^{-ikx} \tag{6.6}$$

At $x = 0$

$$V_T(x=0) = -\frac{P^-}{Z_m} + \frac{P^+}{Z_m} = -\frac{P^-}{Z_m}\left[1 + e^{2ikl}\right] \tag{6.7}$$

At the interface:

$$V_T(x=l) = -\frac{P^-}{Z_m} * e^{ik_l l} + \frac{P^+}{Z_m} * e^{-ik_l l} = -\frac{2P^-}{Z_m} * e^{ik_l l} \tag{6.8}$$

The corresponding gain is obtained by:

$$G_{air} = 20 * \log\left(\frac{V_T(x=l)}{V_0}\right) = 20 * \log\left(\frac{2 * e^{ikl}}{1 + e^{2ikl}}\right) = 20 * \log\left(\frac{1}{\cos(kl)}\right) \tag{6.9}$$

To predict the acoustic pressure that would be produced at 1m in water, the following expression has to be used

$$P_{@1m} = \frac{1}{R} * \frac{G_w(v_{mes})\rho c r_0}{G_{air}\sqrt{1 - \frac{1}{k^2 a^2}}} \tag{6.10}$$

The signal emitted by the accelerometers was passed through a 4 channel ICP® sensor signal conditioner made by PCB (Model 442B104) and numerically registered. Filtering was performed in the same manner as the in-water signals.

The sensitivity of the accelerometer is approximately 10mV/G. The velocity is deduced from

$$v = \frac{a}{2\pi f}, \tag{6.11}$$

where v is the velocity, a is the acceleration and f is the difference frequency.

The influence of the driving voltage transmitted to the source was first studied. Measurements were obtained at a static pressure of 10 PSI and are presented in Fig. 6.10. We can observe that the measured velocity at 300 Hz increase dramatically above a drive voltage of 120 per primary frequency which can probably be explained by the introduction of nonlinearities by the amplifier at high voltage. We then need to restrict our measurements in a voltage range below 120V.

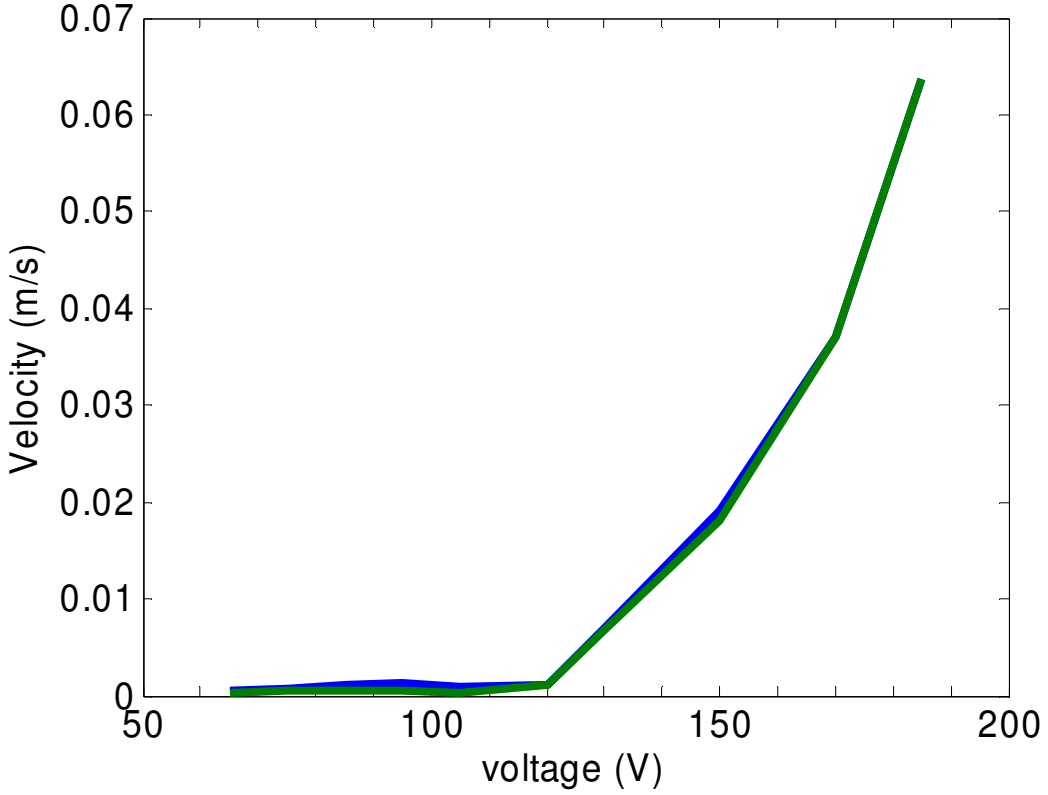

Figure 6.10 Velocity measured by 2 accelerometers in function of the driving voltage at a static pressure of 10 PSI

The influence of the pressure was then studied. A maximum static pressure of 34 PSI was used in the experiment. Measurements were then performed while the pressure decreased. The velocity as a function of the hydrostatic pressure was measured.

The results are compared to the results of the simulation and to the linear response of the source at 300 Hz and the same driving voltage (210 V) (Fig. 6.11).

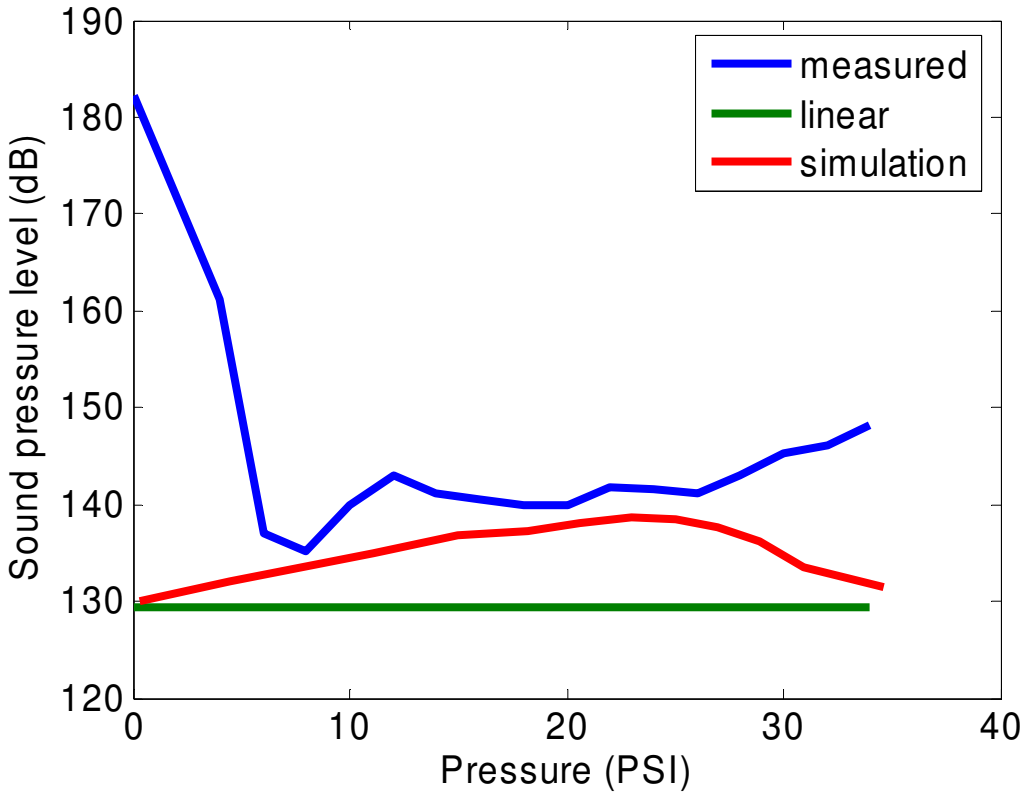

Figure 6.11 Comparison of the signal measured by the accelerometer, the linear level and the simulation

The measurements at very low pressure are unusually high and may explain the fact that higher levels were measured in the water tank at 2m than at higher depths. We suspect that another source of nonlinearity, which is not due to the buckling of the microspheres, is responsible for the large difference frequency signal near ambient static pressure. The measured difference frequency, between 8 and 25 PSI is in reasonable agreement with theory; however, theory and measurement diverge at higher static pressure. To check the homogeneity of the source, measurements on different tiles are performed (Fig 6.12).

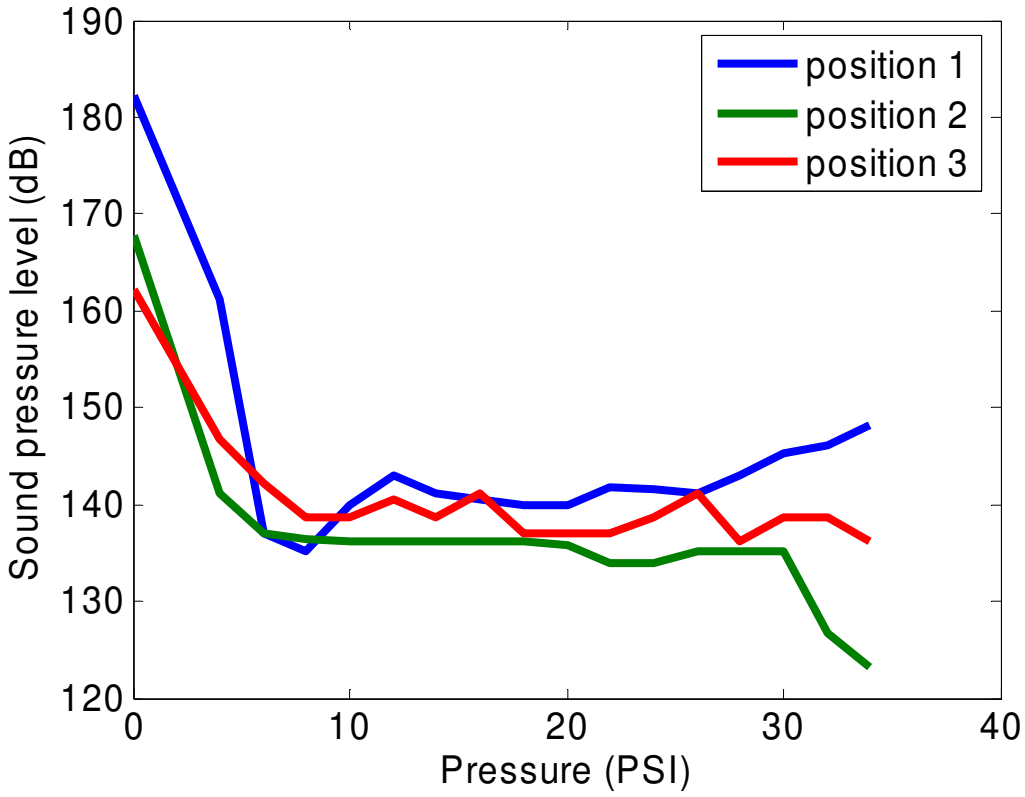

Figure 6.12 Comparison of the measurements of 3 different tiles as a function of the pressure

On the figure 6.12, one can observe differences in the measurements between the different tiles placed in the same conditions. These differences could be explained by the presence of air at the interface piezoelectric shell-tile. Indeed, in the presence of air, the sound wave create by the shell would be scattered and the transmission of energy to the tile would then be affected and would result in a lower velocity of the external surface of the tile. Even considering these differences, the levels obtained in the pressure chamber remain higher than the levels measured in the water tank where the signals measured were not higher than the noise level. This could be explained by the fact that the

measurements were performed at the center of the tiles which is supposed to be the best location whereas signals measured close to the periphery would have maybe been lower. The presence of a high level of difference frequency and therefore high nonlinearities at very low static pressure was not expected and could be explained by the presence of small air bubbles remaining despite the air evacuation. Vibration of these bubbles could create nonlinear effect that disappears with higher pressure because of the crush of the bubbles.

CHAPTER VII

CONCLUSION

7.1 Summary of the work

The goal of the thesis was to optimize the working of an existing compact, omnidirectional, parametric source by redesigning the nonlinear layer that surrounded the linear projector. The existing source had a nonlinear layer composed of a mix of gel with microspheres.

The optimization design consisted of different steps:

-The research on microspheres that buckle at high hydrostatic pressure. The use of smaller microspheres allowed us to go from a 9 PSI to a 20 PSI buckling pressure.

-The investigation of a matrix material which is soft enough to allow microspheres to buckle and solid enough to make the source easy to handle. A 2-part polyurethane has been used.

-The determination of the properties of the nonlinear medium composed of the microspheres and the matrix as a function of static measurements. These measurements provide an estimate of the sound speed and the nonlinear coefficient of the medium.

-The estimation of the efficiency of the medium using a simulation program. The program gave us the particle velocity of the sound wave while this latter propagates through the medium.

-The construction of the nonlinear layer around the source. Tiles composed of the nonlinear medium have been built and adhered to the source.

Measurements have then been achieved, first in a water tank and then in a pressure chamber to validate the predicted behavior of the source.

7.2 Results

Measurements revealed that the behavior of our source was not exactly as expected. Highest levels of difference frequency have been detected at very low hydrostatic pressure whereas our model predicted very low efficiency in this range of pressure. This implies the presence of another source of nonlinearity which is not due to the buckling properties of the microspheres. At higher hydrostatic pressure, our results in the water tank appeared to be lower than expected and lower than the pressure chamber measurements. An explanation is the connection between the source and the tiles. Indeed, if the tiles are not exactly in contact with the source, losses are introduced at the interface.

7.3 Future work

The behavior of the source at very low hydrostatic pressure has to be analyzed to find out an explanation of the unexpected high levels of difference frequency measured.

A way to create a more efficient bond between the source and the nonlinear medium, in order to minimize losses at the interface, has to be studied.

The buckling pressure of the microspheres is still low. To make it higher, microspheres with thicker walls need to be found and tested.

APPENDIX I: NONLINEAR PROPAGATION PROGRAM

```
% Initialization of the variables

J=1500;                                 % Number of harmonics
g(1:J)=0.0000000000;                    % Gk coefficients
g(12)=0.105;
g(13)=0.105;
gx(1:J)=0.0000000000;
g2(1:J)=0.0000000000;
h(1:J)=0.0000000000;                    % Hk coefficients
hx(1:J)=0.0000000000;
h2(1:J)=0.0000000000;
x1(1:J,1:J)=0.0000000000;
x11(1:J,1:J)=0.0000000000;
x2(1:J,1:J)=0.0000000000;
x22(1:J,1:J)=0.0000000000;
freq=300;                               % Difference frequency
c=370.000;                              % Sound speed in the medium
beta=-300.0;                            % Coefficient of nonlinearity
e=1;                                    % Normalization coefficient
dx=0.00625;                             % Stepsize
ro=0.075;                               % Starting distance
deltaC=0;                               % Sound speed step
coef=300;                               % Number of harmonics reduced
```

```
k=2;                                    % Number of initial coefficients
ki=0;

% Computation of the absorption coefficients

alpha(1)=0.03;
for i=2:J
    alpha(i)=i*i*alpha(1);
end

% Computation of the dispersion coefficients

for i=1:J
    delt(i)=(i*freq*2*pi/c)*(1-(c/(c+(i-1)*deltaC)));
end




% Compute the matrix element

b=pi*beta*freq/(c*c);

for id=2:J
    izx=id-1;
    for im=1:izx;
        x11(id,im)=exp((alpha(id)-alpha(im)-alpha(id-im))*dx);
        x1(id,im)=1.00000;
```

```
        end
end
ifx=J-1;
for inn=1:ifx
    inz=J-inn;
    for ip=1:inz;
        x22(inn,ip)=exp((alpha(inn)-alpha(ip)-alpha(inn+ip))*dx);
        x2(inn,ip)=1.00000;
        end
end
gh(1:J)=exp(-alpha(1:J)*dx);
rn=r0;
r=rn;
f1=1.000000000;
a=1;



for iii=1:2000                          % iii = number of steps
r=ro+iii*dx;                            % propagation distance
cb=dx*b*f1;
g2(1:J)=g(1:J);
h2(1:J)=h(1:J);
dg(1:J)=0.0000;
dh(1:J)=0.0000;
dg1(1:J)=0.0000;
dh1(1:J)=0.0000;

% Computation of the first derivative
```

```
    for is=2:J
        ill=is-1;
        for it=1:ill
        cx=cb*it*x1(is,it);
        dg(is)=cx*(g2(is-it)*g2(it)-h2(is-it)*h2(it))+dg(is);
        dh(is)=cx*(h2(is-it)*g2(it)+g2(is-it)*h2(it))+dh(is);
        end
    end
    for iu=1:J
        izz=J-iu;
        for iv=1:izz
        cx=cb*iu*x2(iu,iv);
        dg(iu)=dg(iu)-cx*(g2(iu+iv)*g2(iv)+h2(iu+iv)*h2(iv));
        dh(iu)=dh(iu)+cx*(g2(iu+iv)*h2(iv)-h2(iu+iv)*g2(iv));
        end
    end

% Computation of the new amplitudes for the second derivative

g2(1:J)=g(1:J)+dg(1:J);
h2(1:J)=h(1:J)+dh(1:J);

ii=J-coef;

g2(ii:J)=0.8*g2(ii-1);              % Reduction of the last harmonics
h2(ii:J)=0.8*h2(ii-1);              % Reduction of the last harmonics
r=r+dx;
f1=rn/r;
cb=dx*b*f1;
```

```
% Computation of the second derivative


    for is=2:J
        ill=is-1;
        for it=1:ill
        cx=cb*it*x11(is,it);
        dg1(is)=cx*(g2(is-it)*g2(it)-h2(is-it)*h2(it))+dg1(is);
        dh1(is)=cx*(h2(is-it)*g2(it)+g2(is-it)*h2(it))+dh1(is);
        end
    end
    for iu=1:J
        izz=J-iu;
        for iv=1:izz
        cx=cb*iu*x22(iu,iv);
        dg1(iu)=dg1(iu)-cx*(g2(iu+iv)*g2(iv)+h2(iu+iv)*h2(iv));
        dh1(iu)=dh1(iu)+cx*(g2(iu+iv)*h2(iv)-h2(iu+iv)*g2(iv));
        end
    end


% Computation of the new amplitudes.


g(1:J)=g(1:J)+0.5*(dg(1:J)+dg1(1:J));  %integration thanks to the
h(1:J)=h(1:J)+0.5*(dh(1:J)+dh1(1:J));  %runge-kutta method



g(ii:J)=0.8*g(ii-1);                % Reduction of the last harmonics
h(ii:J)=0.8*h(ii-1);                % Reduction of the last harmonics
```

```
for ix=1:J
        g(ix)=g(ix)*f1*gh(ix);
        h(ix)=h(ix)*f1*gh(ix);
end

% Introduction of the dispersion

for i=1:J
    a1=g(i);
    b1=h(i);
    c1=delt(i);
    g(i)=(a1*cos(c1*dx)+b1*sin(c1*dx));
    h(i)=(b1*cos(c1*dx)-a1*sin(c1*dx));
end
    rn=r;
    r
    g(1)
    se=[];
    fido=fopen('fundamental.txt','w');
    fprintf(fido,'%f ',g);
    fprintf(fido,'\n',se);
    fclose(fido);

% Recording of the coefficients in text files

    if (mod(iii,10)==0)
        fid1=fopen('CosNumEnd.txt','w');
        fid2=fopen('SinNumEnd.txt','w');
        for (i=1:J)
```

```
        fprintf(fid1,'%1.10f\n',h(i));
        fprintf(fid2,'%1.10f\n',g(i));
        end
        fprintf(fid1,'%1.10f\n',r);
        fprintf(fid2,'%1.10f\n',r);
   st1=fclose(fid1);
   st2=fclose(fid2);
    end

end
```

APPENDIX II: Microsphere properties

www.Expancel.com

EXPANCEL® DE

Product Specification

Dry Expanded Microspheres

Packed in cartons with 1, 4, 5 or 6 polyethelene bags,
e g 4x5 kg **EXPANCEL 551 DE 40 d42**.
Volume of carton 1.15 m³, incl pallet

EXPANCEL	Particle Size µm[1] D(0.5)	True Density, kg/m³ [2]	Solvent Resistance [3]
551 DE 40 d42	30 - 50	42 ± 4	* * *
551 DE 20 d60	18 - 28	60 ± 5	* * *
551 DE 80 d42	50 - 80	42 ± 4	* * *
461 DE 20 d70	15 - 25	70 ± 6	* * * *
461 DE 40 d25	35 - 55	25 ± 3	* * * *
461 DE 40 d60	20 - 40	60 ± 5	* * * *
461 DET 40 d25	35 - 55	25 ± 3	* * * *
051 DE 40 d60	20 - 40	60 ± 5	* * * *
091 DE 40 d30	35 - 55	30 ± 3	* * * * *
091 DE 80 d30	60 - 90	30 ± 3	* * * * *

Not all grades available in all locations. Check local sales office for availability.

(1) Technical Bulletin no 8b
(2) Technical Bulletin no 26
(3) Technical Bulletin no 10

AKZO NOBEL

Head Office: Expancel, PO Box 13000, SE-850 13 Sundsvall, SWEDEN, Phone: +46 60 13 40 00, Fax: +46 60 56 95 18
US Office: Expancel Inc, 2240 Northmont Pkwy, Duluth, GA 30096, USA, Phone: +1 770 813 9126, Fax: +1 770 813 8639
E-mail: info@expancel.com Internet: www.Expancel.com
Issue 2005.11 (Replaces 2005.08)

APPENDIX III: Polyurethane elastomer specifications

BJB ENTERPRISES, INC.

F-15 A/B
15 SHORE A CASTABLE POLYURETHANE ELASTOMER

PRODUCT HIGHLIGHTS:

- Resists moisture absorption
- Very easy to use
- Cures at room temperature
- Highly resilient, tough, stretchy and tack free
- Quick demold time, low viscosity

PHYSICAL PROPERTIES:

Hardness, Shore A ASTM D-2240	15 ± 2
Density, (g/cc) ASTM D-792	1.00
Cubic Inches Per Pound	27.7
Color/Appearance	Light amber, transparent-clear
Tensile Strength, (psi) ASTM D-412	240
Elongation, (%) ASTM D-412	850
Tear Strength, (pli) ASTM D-624	25
Shrinkage, (in./in.) linear ASTM D-2566	0.008

HANDLING PROPERTIES:

Mix Ratio (by weight):	
Part A	45 parts by weight
Part B	100 parts by weight
Mix Ratio (by volume):	
Part A	42 parts by volume
Part B	100 parts by volume
Specific Gravity:	
Part A	1.05
Part B	0.98
Viscosity, (cps) @ 77°F (25°C) Brookfield:	
Part A	3,700
Part B	70
Mixed	275
Work Time, (100-gram mass) @ 77°F (25°C)	20-25 minutes
Demold Time @ 77°F (25°C)	2-3 hours (See NOTE)

CURE SCHEDULE/HEAT CURING:

Most of the physical properties can be achieved in 5-7 days at ambient temperature, 77°F (25°C). In order to achieve maximum physical properties, a post cure with heat is required. BJB recommends 24 hours at ambient temperature, 77°F (25°C), followed by 16 hours at 160°F (71°C).

For more information call BJB Enterprises, Inc. (714) 734-8450 Fax (714) 734-8929

MOLD PREPARATION AND RELEASING:

When F-15 A/B is used to reproduce molds from plaster, wood or other porous substrates, we would first recommend that they be sealed. Release agents may then be applied over the sealed surface.

MIXING:

Mix thoroughly, being sure to scrape sides and corners of containers so no unmixed material remains. Vacuum degassing is important to achieving an air free product. To aid the evacuation of air, the use of a surface tension reducing agent, such as BJB's AF-4, is necessary. Refer to BJB polyurethane handling guide and data on AF-4 for additional information.

NOTE:

Demold times can be reduced with a mild post-cure at elevated temperatures of 130° - 160°F (54° - 71°C). Prolonged direct exposure to sunlight can affect the surface of this product. Cover molds or other products when storing outdoors. **The cure will be inhibited if cast against a tin catalyzed silicone RTV.**

STORAGE:

Maintain at 77° ± 15°F (25° ± 10°C) and use a dry inert gas prior to sealing containers. Shelf life is 6 months from date of shipment in unopened containers.

PACKAGING:

Gallon kits	3.6 lbs. A, 8 lbs. B
5 Gallon kits	18 lbs. A, 40 lbs. B
Drum kits	180 lbs. A, 400 lbs. B

SAFETY PRECAUTIONS:

Use in a well-ventilated area. Avoid contact with skin using protective gloves and protective clothing. Repeated or prolonged contact on the skin may cause and allergic reaction.

Eye protection is extremely important. Always use approved safety glasses or goggles when handling this product.

IF CONTACT OCCURS:

Skin: Immediately wash with soap and water. Remove contaminated clothing and launder before reuse. It is *not* recommended to remove resin from skin with solvents. Solvents only increase contact and dry skin. Seek qualified medical attention if allergic reactions occur.

Eyes: Immediately flush with water for at least 15 minutes. Call a physician.

Ingestion: If swallowed, call a physician immediately. Remove stomach contents by gastric suction or induce vomiting only as directed by medical personnel. Never give anything by mouth to an unconscious person.

Refer to the Material Safety Data Sheet before using this product.

For more information call BJB Enterprises, Inc. (714) 734-8450 Fax (714) 734-8929

APPENDIX IV: Tile technical drawings

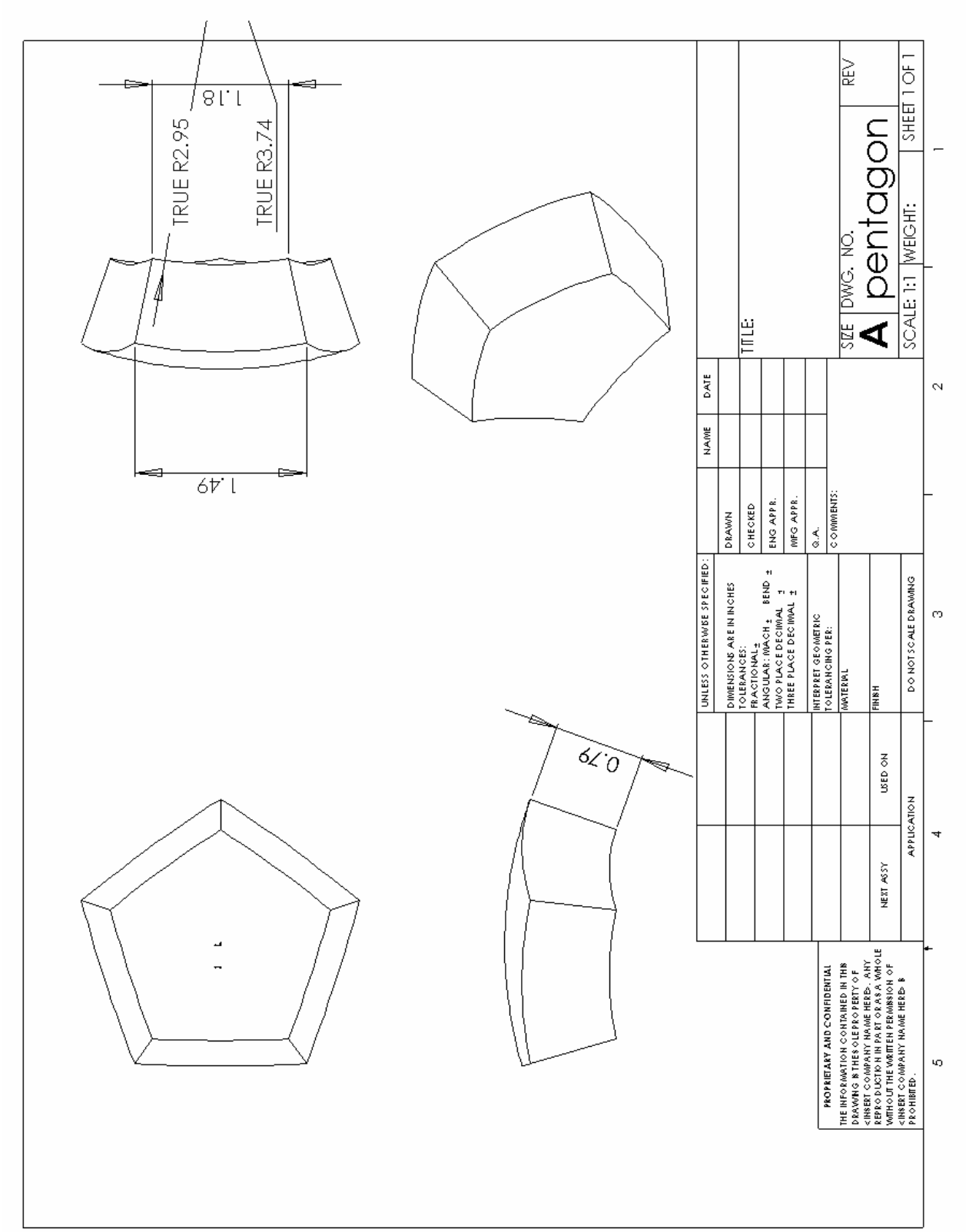

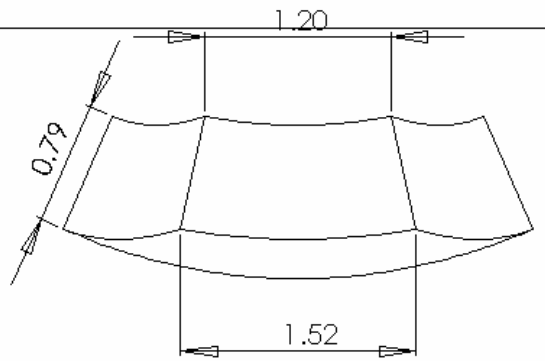

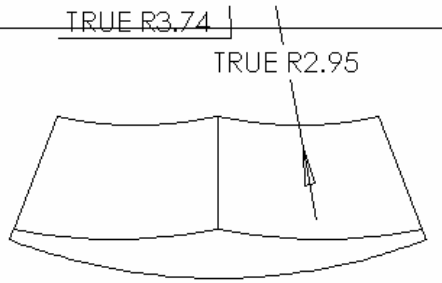

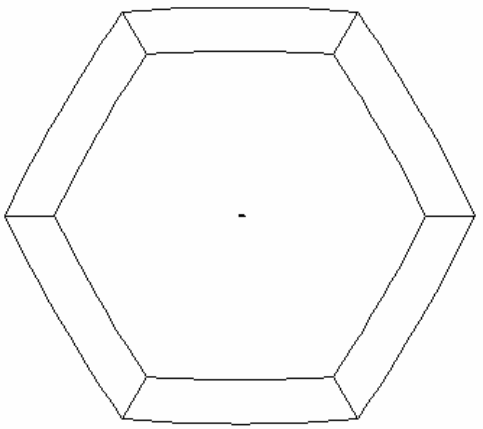

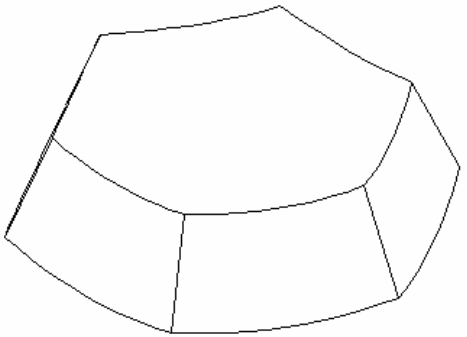

		UNLESS OTHERWISE SPECIFIED:		NAME	DATE
		DIMENSIONS ARE IN INCHES TOLERANCES: FRACTIONAL ± ANGULAR: MACH ± BEND ± TWO PLACE DECIMAL ± THREE PLACE DECIMAL ±	DRAWN		
			CHECKED		
			ENG APPR.		
			MFG APPR.		
		INTERPRET GEOMETRIC TOLERANCING PER:	Q.A.		
		MATERIAL	COMMENTS:		
NEXT ASSY	USED ON	FINISH			
APPLICATION		DO NOT SCALE DRAWING			

PROPRIETARY AND CONFIDENTIAL

THE INFORMATION CONTAINED IN THIS DRAWING IS THE SOLE PROPERTY OF <INSERT COMPANY NAME HERE>. ANY REPRODUCTION IN PART OR AS A WHOLE WITHOUT THE WRITTEN PERMISSION OF <INSERT COMPANY NAME HERE> IS PROHIBITED.

TITLE:

SIZE	DWG. NO.	REV
A	hexagon	
SCALE: 1:1	WEIGHT:	SHEET 1 OF 1

5 4 3 2 1

APPENDIX V: Hydrophone calibration

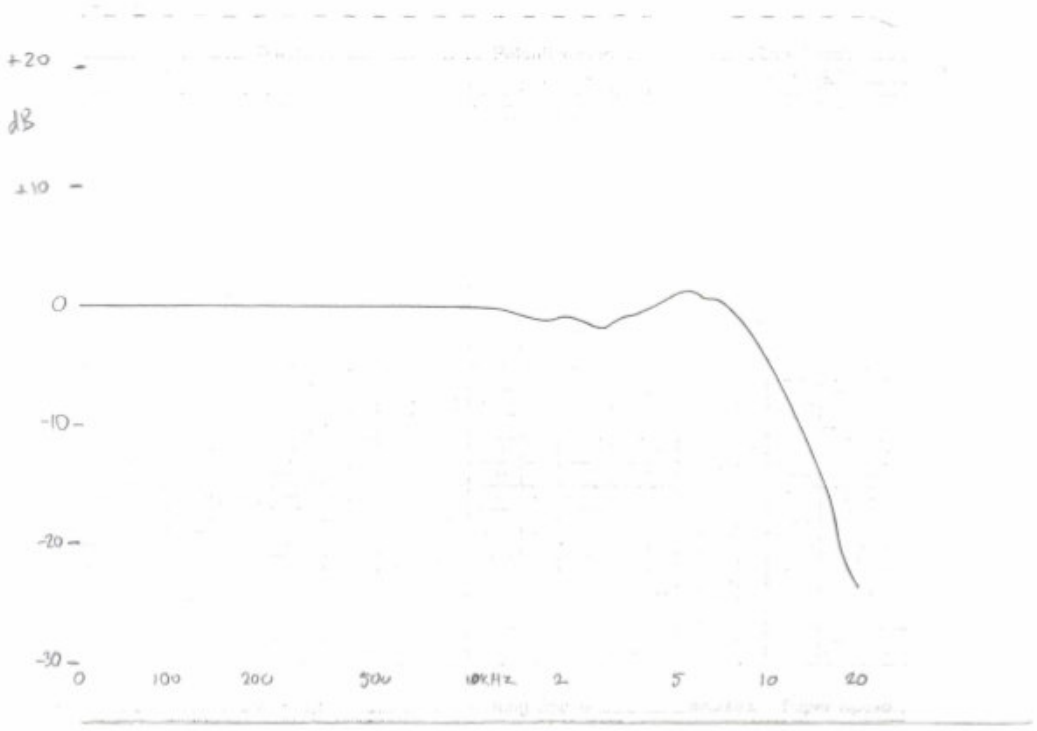

Calibration Chart for Hydrophone Type 8100

Brüel & Kjær

Serial No. 1112103

Reference Sensitivity at 250 **Hz*at** 23 **°C**
including 7,2 m cable

Cable Capacitance 100 pF/m typical

Open Circuit Sensitivity:

Voltage Sensitivity:

-205,8 dB re 1 V/µPa**

-85,8 dB re 1 V per Pa or 57,3 µV per Pa

-105,8 dB re 1 V per µbar**

Charge **Sensitivity:** 416 · 10⁻³ pC per Pa

Capacitance (including 7,2 m cable) 8100 pF

Frequency Response:
Individual Free Field Frequency Response Curve attached.

Date 84.03.14. **Signature** [signature]

Summarized Specifications:

Usable Frequency Range: 0,1 Hz to 125 kHz (—10 dB)

Linear Frequency Range:
0,1 Hz to 10 kHz ± 1 dB
0,1 Hz to 50 kHz ± 2 dB

Horizontal Directivity 100 kHz: (XY-plane) typical ± 2 dB

Physical:

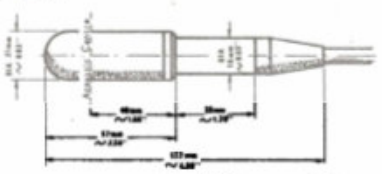

Leakage Resistance: 71 · 10⁴ MΩ at 23 °C

Operating Temperature Range:
—40°C to + 120°C
—40°F to + 248°F

Change of Sensitivity with Temperature:
Voltage —0,04 dB/°C
Charge + 0,03 dB/°C

Change of Sensitivity with Static Pressure:
—3 × 10⁻⁷ dB/Pa (—0,03 dB/ato)

Temperature Transient Sensitivity:
< 70 Pa/°C (< 0,7 mbar/°C)
(ANSI S.2.11-1969); measured with B & K Charge Preamplifier Type 2626, LLF 3 Hz

Maximum Operating Static Pressure:
40 ato (400 m or 1200 ft ocean depth)

Cable:
Two conductors shielded low noise, low capacitance
Waterblocked to MIL 915 A
Extention cables available

Weight including 7,2 m cable with waterproof extension connector:
1,3 kg

APPENDIX VI: Transducer TVR

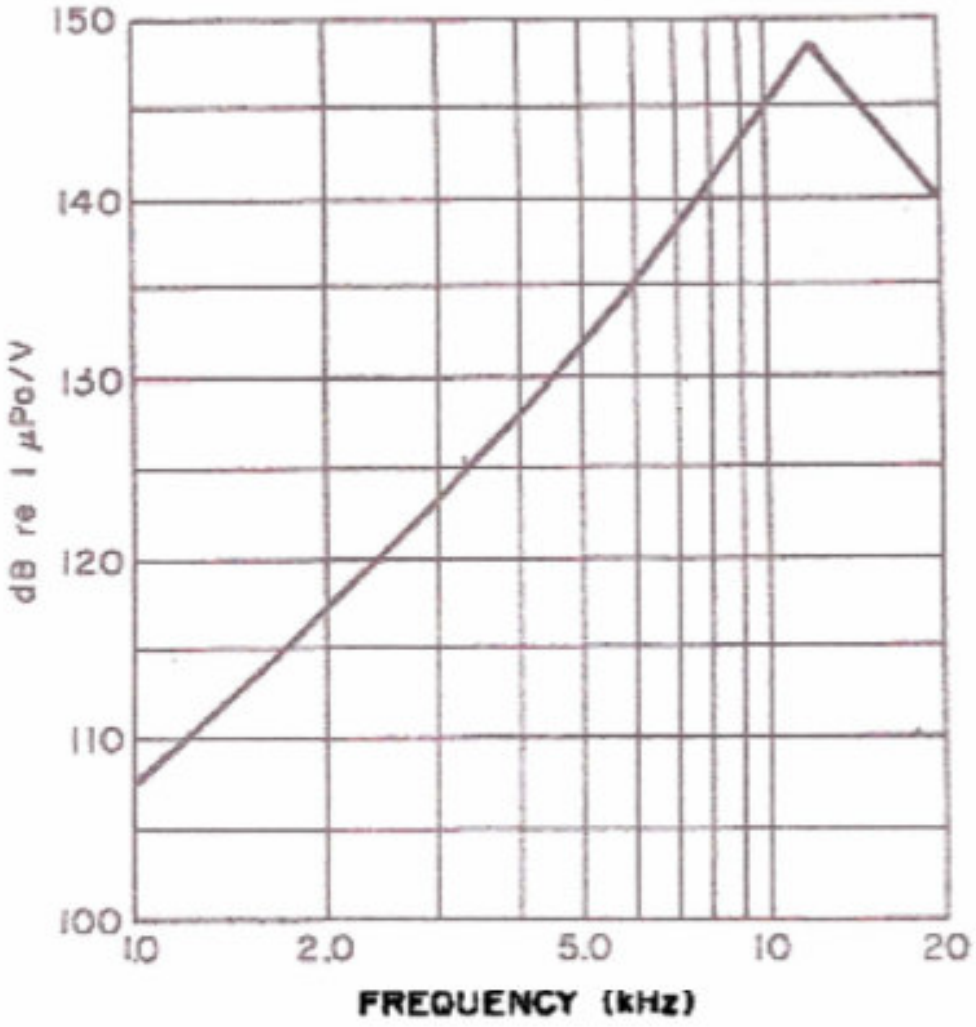

Typical Transmitting Voltage Response for

Type F56 transducer

References

[1] P. J. Westervelt, *Parametric acoustic array*, J.Acoust. Soc. Am. **35**, 535-537, 1963

[2] H. O. Berktay, *Possible exploitation of non-linear acoustics in underwater transmitting applications*, J. Sound Vib., **2**, 435-461, 1965

[3] T. G. Muir and J.G. Willette, *Parametric acoustic transmitting arrays*, J. Acoust. Soc. Am. **52**, 1481-1486, 1972

[4] H.C. Woodsum, *Enhancement of parametric efficiency by saturation suppression*, J. Sound Vib., **69**, 27-33, 1980

[5] L. Kustov, V. Nazarov, L. Ostrovsky, A. Sutin and S.Zamolin, *Parametric acoustic radiator with a bubble layer*, Acous. Lett. , Vol. 6, 2, 1982

[6] Kozyaev and Naugol'nykh, *Parametric sound radiation in a two-phase medium*, Sov. Phys. Acoust. **26**, 48-51, 1980

[7] A.L. Polyakova and O.Yu. Sil'vestrova, *Parametric radiator operating in a medium containing gas bubbles*, Sov. Phys. Acoust. **26**, 441-443, 1980

[8] Yu. A. Kobelev and A. M. Sutin, *Difference-frequency sound generation in a liquid containing bubbles of different sizes*, Sov. Phys. Acoust. **26**, 485-487, 1980

[9] Oleg A. Druzhinin, Lev A. Ostrovsky ad Andrea Prosperetti, *Low-frequency acoustic wave generation in a resonant bubble layer*, J. Acoust. Soc. Am. **100** (6), 3570-3580, 1996

[10] J. Wu and Z. Zhu, *Measurements of the effective nonlinearity parameter B/A of water containing trapped cylindrical bubbles*, J. Acoust. Soc. Am. **89** (6), 2634-2639, 1991

[11] T. Asada and Y. Watanabe, *Stable Parametric Amplification Using Elastic Microcapsules Placed in Silicone Rubber*, Jap J. Appl. Phys., **30**, suppl.30-1,57-59, 1991

[12] S. N. Gurbatov, *Parametric interaction and amplification of random waves in a nondispersive medium*, Sov. Phys. Acoust. **26**, 302-307, 1980

[13] I. V. Khazanov, *Nonlinear wave interactions in an acoustic resonator*, Sov. Phys. Acoust. **26**, 447-450, 1980

[14] K. Hashiba and H. Masuzawa, *Effect of Micro-Bubbles in Water on Beam Patterns of Parametric Array*, Jap J. Appl. Phys., **42**, 3227-3232, 2003

[15] D. H. Trivett and A. L. Van Buren, *A Fortran computer program for calculating the propagation of plane, cylindrical, or spherical finite amplitude waves*, 1981

[16] D. H. Trivett and A. L. Van Buren, *Propagation of plane, cylindrical and spherical finite amplitude waves*, J. Acoust. Soc. Am. **69**, 943-949, 1981

[17] Lev A. Ostrovsky, A. M. Sutin, I. A. Soustova, A. I. Mateyev, and A. I. Potapov, *Nonlinear, low-frequency sound generation in a bubble layer: Theory and laboratory experiment*, J. Acoust. Soc. Am. **104**, Issue 2, 722-726, 1998

[18] C. M. Hedberg, *Nonlinear propagation through a fluid of waves originating from a biharmonic sound source*, J. Acoust. Soc. Am. **96**, 1821-1828, 1994

[19] T. G. Muir and L.L. Mellenbruch, *Reflection of finite-amplitude waves in a parametric array*, J. Acoust. Soc. Am., **62**, No. 2, 271-276, 1977

[20] B. E. McDonald and W. A. Kuperman, *Time-domain formulation for pulse propagation including nonlinear behavior at a caustic,* J. Acoust. Soc. Am. **81**, 1406–1417, 1987

[21] K. Castor, P. Gerstoft, P. Roux, B. E. McDonald, and W. A. Kuperman, *Long-range propagation of finite-amplitude acoustic waves in an ocean waveguide,* J. Acoust. Soc. Am. **116**, Issue, 2004-2010, 2004

[22] D.H.Trivett, H. Pinçon and P. H. Rogers, *Investigation of a three-phase medium with a negative parameter of nonlinearity*, received for publication in J. Acoust. Soc. Am

[23] H. Pinçon, *Investigation of a medium with a negative coefficient of nonlinearity*, Master thesis, Georgia Inst. of Tech., 2002

[24] O. Pauly, *Characterization of three phase medium with a large and negative parameter of nonlinearity*, Master thesis, Georgia Inst. of Tech., 2003

[25] A. Dumortier, *Investigation of a medium with a large, negative parameter of nonlinearity and its application to the enhancement of a compact, omnidirectional, parametric source*, Master thesis, Georgia Inst. of Tech., 2004

[26] J. Marchal, *Acoustique non lineaire : Contribution theorique et experimentale a l'etude de l'emission parametrique (nonlinear acoustics : theoritical and experimental contribution to parametric transmission)*, These, Universite Paris 6, 2002

[27] R. T. Beyer, *Nonlinear Acoustics*, 1974

[28] B. O. Enflo and C. M. Hedberg, *Theory of Nonlinear Acoustics in Fluids*, 2002

[29] K. Naugolnykh and L. Ostrovsky, *Nonlinear Wave Processes in Acoustics*, 1998

[30] B.K. Novikov, O.V. Rudenko and V.I. Timoshenko, *Nonlinear Underwater Acoustics*, 1981

[31] S.C. Chapra, R.P. Canal, *Numerical methods for engineers*, 1998